A phosphatase-centric mechanism drives stress signaling response

David Maria Hollenstein[1],[†] , Gabriela Gérecová[1],[†] , Natalie Romanov[2] , Jessica Ferrari[1],
Jiri Veis[1,3] , Marion Janschitz[1] , Reinhard Beyer[4,5] , Christoph Schüller[4,5] , Egon Ogris[3] ,
Markus Hartl[1,6] , Gustav Ammerer[1] & Wolfgang Reiter[1,6,*]

Abstract

Changing environmental cues lead to the adjustment of cellular physiology by phosphorylation signaling networks that typically center around kinases as active effectors and phosphatases as antagonistic elements. Here, we report a signaling mechanism that reverses this principle. Using the hyperosmotic stress response in *Saccharomyces cerevisiae* as a model system, we find that a phosphatase-driven mechanism causes induction of phosphorylation. The key activating step that triggers this phospho-proteomic response is the Endosulfine-mediated inhibition of protein phosphatase 2A-Cdc55 (PP2A^{Cdc55}), while we do not observe concurrent kinase activation. In fact, many of the stress-induced phosphorylation sites appear to be direct substrates of the phosphatase, rendering PP2A^{Cdc55} the main downstream effector of a signaling response that operates in parallel and independent of the well-established kinase-centric stress signaling pathways. This response affects multiple cellular processes and is required for stress survival. Our results demonstrate how a phosphatase can assume the role of active downstream effectors during signaling and allow re-evaluating the impact of phosphatases on shaping the phosphorylome.

Introduction

Cells respond to external and internal stimuli by activation of complex signaling networks that are typically characterized by highly conserved, intertwined signaling pathways. Both signal propagation and the eventual integration mechanisms need to be fine-tuned for the cell to adequately respond to specific situations. The most common mechanism by which a signal is transmitted within the cell is reversible protein phosphorylation. The addition and removal of the phosphate moiety can modulate protein functionality, as well as its activity, localization, and protein interactions. Dysregulation of signaling networks, i.e., perturbations of the phosphorylome, can have disastrous consequences and represent hallmarks of many diseases (Grundke-Iqbal *et al*, 1986; Meyerovitch *et al*, 1989; Blume-Jensen & Hunter, 2001; Eidenmüller *et al*, 2001; Ozcan *et al*, 2004; Rikova *et al*, 2007; Zanivan *et al*, 2013). It is therefore pivotal to investigate phosphorylation and its effects on regulatory networks to fully understand cell behavior, as well as health and disease.

In human cells, up to 65% of expressed proteins get phosphorylated (Keshava Prasad *et al*, 2009; Vlastaridis *et al*, 2017; Yu *et al*, 2019), with more than 100,000 distinct phosphorylation events recorded (Vlastaridis *et al*, 2017; Needham *et al*, 2019). However, the regulatory underpinning of 95% of the phosphorylome is still unknown (Needham *et al*, 2019). Almost all efforts to explain the regulation of phosphorylation are centered around protein kinases, directing our understanding of signaling pathways toward a kinase-centric view.

The contribution of protein phosphatases in defining the state of the phosphorylome, on the other hand, has largely not been investigated in-depth. This is due to the fact that phosphatases have been less studied than kinases overall and are typically not considered to be effector proteins of signaling networks (Brautigan, 2013; Smoly *et al*, 2017). The majority of studies highlight a rather passive role of phosphatases in terminating signaling responses or in counteracting a kinase signaling cascade. However, increasing evidence suggests an intricate regulation of activity and composition of protein phosphatase complexes and a highly specific substrate recognition (Virshup & Shenolikar, 2009; Mishra *et al*, 2017; Courtney & Deiters, 2019). It is therefore plausible to assume that

phosphatases could be more actively and specifically involved in determining the state of the phosphorylome.

Here, we report such an active role for the protein phosphatase 2A (PP2A) in the hyperosmotic stress response of *Saccharomyces cerevisiae,* a paradigm signaling response (Hohmann, 2002; Saito & Posas, 2012; Brewster & Gustin, 2014). PP2A, one of the most prominent protein phosphatases, is highly conserved among eukaryotes and has been associated with key cellular processes, such as cell cycle progression, apoptosis, cellular metabolism, and migration (Wlodarchak & Xing, 2016; Ferrari *et al*, 2017; Fabbrizi *et al*, 2018). The PP2A holo-enzyme is a multi-protein complex, consisting of a catalytic, a scaffolding, and a regulatory subunit. Substrate specificity is defined by the so-called regulatory B subunits, in yeast named Cdc55 and Rts1 (Shu *et al*, 1997; Zhao *et al*, 1997; Wu *et al*, 2000; Wei *et al*, 2001; Yabe *et al*, 2018; Játiva *et al*, 2019).

In this study, we reveal a phosphatase-centric signaling response based on the inhibition of PP2A^{Cdc55}, triggering a wide range of stress-induced phosphorylations that in unstressed conditions are kept at a low level by PP2A^{Cdc55}. The inhibition of PP2A^{Cdc55} works through a conserved module composed of the Greatwall Kinase Rim15 and the Endosulfines Igo1 and Igo2, which represent specific inhibitors of PP2A (Gharbi-Ayachi *et al*, 2010; Mochida *et al*, 2010). Phosphorylation of Igo1 and Igo2 by Rim15 promotes their binding to PP2A^{Cdc55}, which results in inhibition of the phosphatase by a mechanism termed unfair competition (Williams *et al*, 2014; Thai *et al*, 2017). Our results suggest that a substantial set of stress-induced phosphorylation sites is affected by the phosphatase in a direct manner, rendering the phosphatase a main downstream signaling effector of the stress response. This phosphatase-driven pathway operates in parallel to and independent of the well-established MAP kinase signaling pathway that is generally considered to be the main regulator of hyperosmotic stress signaling in yeast (Hohmann, 2002; Saito & Posas, 2012; Brewster & Gustin, 2014). The PP2A^{Cdc55} signaling response is essential for stress survival and required for efficient transcription of stress-associated genes. Our findings therefore point toward an unexpected signaling mechanism, based on the inhibition of a phosphatase instead of activation of a kinase as the central effector component of a stress-induced signal transduction pathway.

Results

Identification of the PP2A-affected phosphorylome

Cdc55 and Rts1, the two regulatory subunits of the yeast phosphatase PP2A, have been previously linked to the hyperosmotic stress response (Evangelista *et al*, 1996; Zhao *et al*, 1997; Santhanam *et al*, 2004; Reiter *et al*, 2013). However, the extent to which protein phosphorylation patterns are globally affected by both, PP2A activity and hyperosmotic stress signaling, has not been analyzed before. Here, we used an unbiased mass spectrometry (MS) setup to capture a comprehensive set of potential PP2A substrates exhibiting altered phosphorylation patterns upon hyperosmotic stress. These were followed up through further biochemical validation (Fig 1, Table EV1).

We first performed large-scale SILAC-based quantitative MS experiments (Ficarro *et al*, 2002; Ong *et al*, 2002) assessing the

impact of a *cdc55Δ* deletion mutant on the phosphoproteome, further referred to as setup *cdc55Δ* (Fig EV1A). In a parallel study (preprint: Hollenstein *et al*, 2020), we conducted similar experiments with cells lacking Rts1, designated as setup *rts1Δ*. The reproducibility of the SILAC ratios for the phosphorylation sites demonstrates the quality and consistency of the MS datasets (Fig EV1B and Appendix Fig S1, see also Methods—"MS study design"). Setup *cdc55Δ* encompassed 51 liquid chromatography (LC)-MS-runs, quantifying 10,790 phosphorylation sites (Dataset EV1). To identify phosphorylation sites that were up- or downregulated, we applied a twofold cutoff. 22.1% of the phosphorylation sites showed an increase in the deletion mutant, whereas only 4.3% showed a decrease and 73.6% remained static (Fig EV1C). Thus, most of the affected sites were prone to become increasingly phosphorylated, which is consistent with the expected impact of phosphatase inactivation. Our dataset also recovered findings from previous *CDC55* deletion studies as we found a multitude of known PP2A^{Cdc55} substrates to be increasingly phosphorylated, such as Sic1 (Moreno-Torres *et al*, 2015), Gis1 (Bontron *et al*, 2013), Net1 (Queralt *et al*, 2006; Wang & Ng, 2006), Mih1 (Minshull *et al*, 1996; Wang & Burke, 1997), Swe1 (Minshull *et al*, 1996; Wang & Burke, 1997), Sli15 (Godfrey *et al*, 2017), and Ndd1 (Godfrey *et al*, 2017).

PP2A^{Cdc55} signaling is central in shaping the phosphorylome during hyperosmotic stress

To elucidate the contribution of PP2A to the hyperosmotic stress response, we compared changes in the phosphoproteome observed in the setups *cdc55Δ* and *rts1Δ* (preprint: Hollenstein *et al*, 2020) with published MS datasets capturing phosphorylation changes during the early response to hyperosmotic conditions (Romanov *et al*, 2017; Data ref: Romanov *et al*, 2017) (Fig 1). The stress dataset, denoted as setup *stress response (SR)*, showed a considerable overlap of quantified phosphorylation sites with the *cdc55Δ* (4,962 unique sites) and *rts1Δ* (3,770 unique sites) MS experiments, allowing an integrative analysis.

First, we examined whether hyperosmotic stress and loss of PP2A activity affect overlapping sets of phosphorylation sites. Indeed, 52.8 and 25.2% of all phosphorylation sites with an increased abundance upon hyperosmotic stress treatment also showed an increase in *cdc55Δ* and *rts1Δ* cells, respectively, indicating that several cellular functions might be commonly affected by hyperosmotic stress and PP2A activity (Fig 2A and 2B). Conversely, we could not detect an apparent connection between loss of PP2A and phosphorylation sites that were negatively affected by stress exposure. These results indicate that PP2A activity might oppose hyperosmotic stress signaling.

Next, we investigated whether PP2A^{Cdc55} and PP2A^{Rts1} affect similar or distinct parts of the stress-dependent phosphorylome. We compared SILAC ratios of stress-induced phosphorylation sites between setups *cdc55Δ* and *rts1Δ* (Fig EV1D). Of the 211 stress-induced sites that showed Cdc55 or Rts1 dependency, only 34 (16%) were similarly affected by deletion of the individual regulatory subunits, suggesting different roles for the two PP2A complexes in response to high osmolarity conditions.

Despite its central role in hyperosmotic stress, the mitogen-activated protein kinase (MAPK) Hog1 regulates only one third of
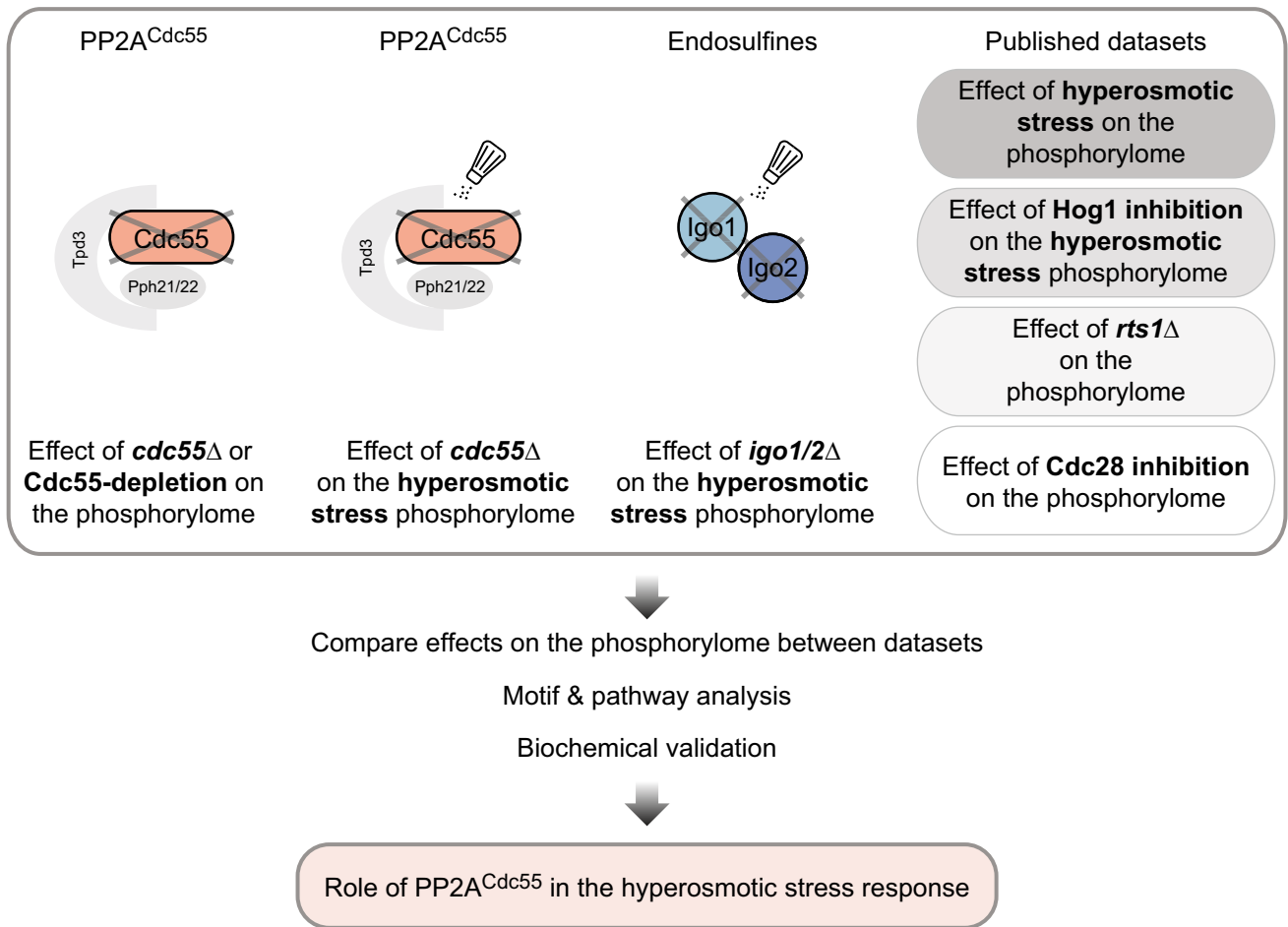
Figure 1. Experimental design to identify PP2A^{Cdc55} effects on the yeast phosphoproteome upon hyperosmotic stress.

Quantitative MS-based phospho-proteomic experiments used in this study. Experiments performed in this study compared the phosphoproteome of a wild-type and a *CDC55* deletion ($n = 8$) or depletion strain ($n = 4$), and the effect of hyperosmotic stress (0.5 M NaCl, 10 min) on global phosphorylation patterns between a wild-type strain and a *CDC55* ($n = 2$) or an *IGO1/IGO1* deletion ($n = 3$) strain. Published MS datasets that were integrated (indicated in the upper right) capture the early response to hyperosmotic stress (0.5 M NaCl, 5 min), and the effect of Hog1 inhibition on the early response to hyperosmotic stress (0.5 M NaCl, 5 min) (Romanov *et al*, 2017; Data ref: Romanov *et al*, 2017), the effect of a deletion of *RTS1* (preprint: Hollenstein *et al*, 2020) and the effect of Cdc28 inhibition (Kanshin *et al*, 2017) on the global phosphoproteome. All SILAC ratios represent knockout versus wild-type, stressed versus unstressed, or inhibited versus not inhibited. After integration of the datasets, further analyses were performed using motif & GO enrichment, as well as *in vivo* biochemical validation.

Figure 2. Deletion of Cdc55 affects phosphorylome at the onset of hyperosmotic stress.

A   Scatter plot displaying log2 SILAC ratios of individual phosphorylation sites in the experiment setup SR on the *y*-axis and setup *cdc55Δ* on the *x*-axis. Black dots represent Hog1-dependent sites [ratio in setup SR ≥ 2 and affected by Hog1as inhibition (ratio ≤ 0.5)] (Romanov *et al*, 2017).

B   Histogram displaying the SILAC ratios (log2) of stress-induced phosphorylation sites in setup *cdc55Δ* (upper panel) and setup *rts1Δ* (lower panel) (preprint: Hollenstein *et al*, 2020), stratified by their Hog1 dependence (gray area versus thick black line).

C   Schematic illustration of suggested model of Cdc55 regulation in the hyperosmotic stress response, with gray arrows signifying hypothetical relationships.

D   Line plot monitoring growth rate (*y*-axis) of indicated strains (colored lines) under different osmolarity conditions (*x*-axis).

E   Histogram displaying the SILAC ratios (log2) of stress-induced phosphorylation sites that are induced in setup *cdc55Δ* in two separate experiments. The blue histogram shows the distribution of fold-changes when *IGO1* and *IGO2* are deleted and cells are exposed to hyperosmotic stress (setup SR *igo1Δigo2Δ*). The orange histogram shows the distribution of fold-changes after deletion of *CDC55* and upon exposure to hyperosmotic stress (setup SR *cdc55Δ*). The same set of sites was compared between the two experiments.

F   Scatter plot displaying log2 SILAC ratios of phosphorylation sites in the experiment setup SR on the *x*-axis and setup SR *igo1Δigo2Δ* on the *y*-axis. Phosphorylation sites that do not exhibit Cdc55 dependence are shown in gray, whereas Cdc55-dependent phosphorylation sites are highlighted in orange. We found an enrichment for Cdc55-dependent sites in the SR- and Igo1/Igo2-dependent set (Set1) (Fisher's exact test, *P*-value = 3.54×10^{-31}, odds ratio = 21.40).

G   Waffle plot showing the impact of different signaling mechanisms on the stress phosphoproteome. Each box corresponds to 1% of the entire set. Orange boxes represent the percentage of phosphosites regulated by PP2A^{Cdc55}, whereas gray boxes represent phosphosites regulated by Hog1 and downstream of the MAPK. Light purple boxes indicate the phosphosites that are neither regulated by Hog1 nor PP2A^{Cdc55}. Dependency was defined as log2 SILAC ratio below −1 or above 1. Rck2 dependency was extracted from Ref. (preprint: Hollenstein *et al*, 2020).
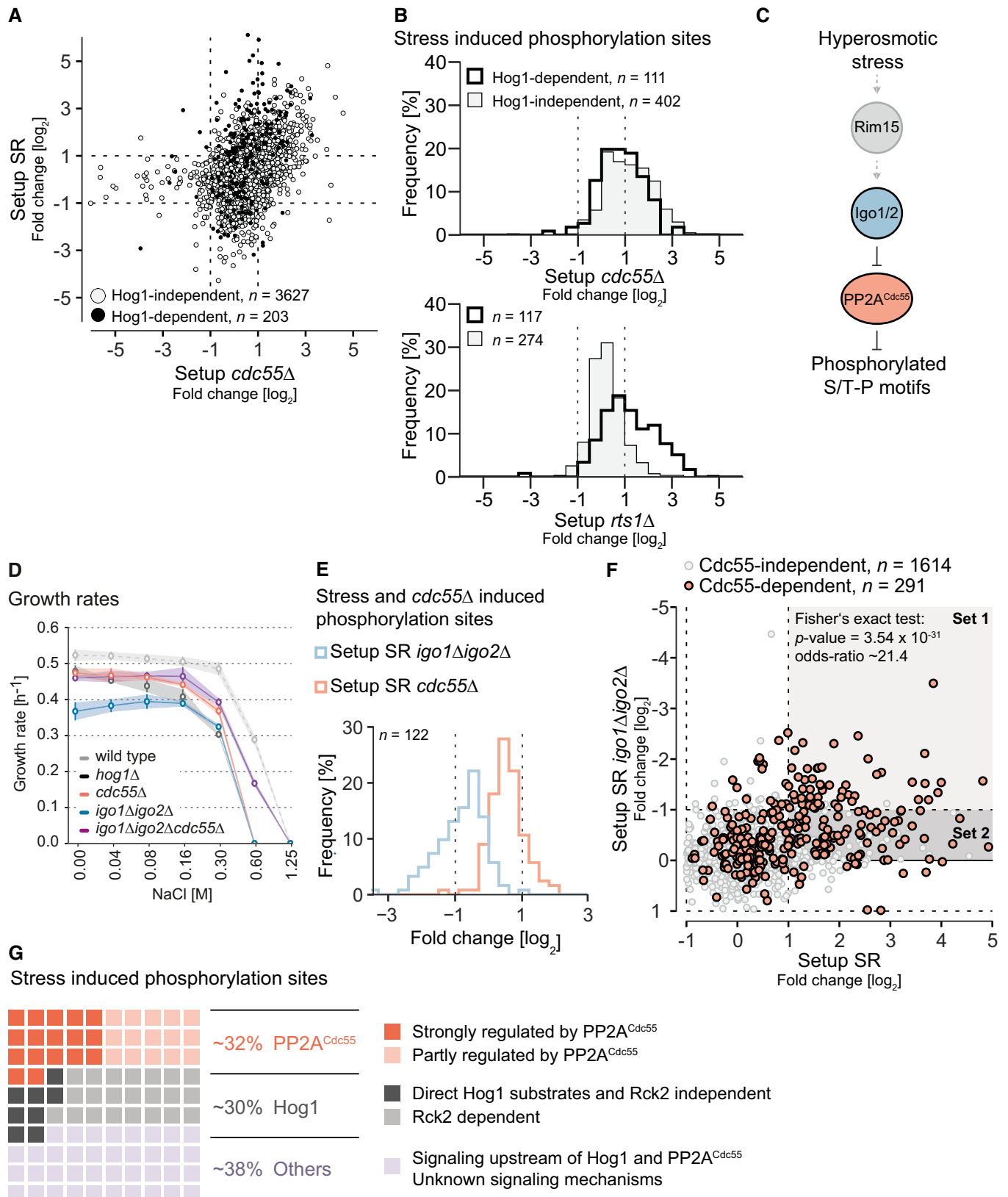
Figure 2.

the stress-dependent phosphorylome (Romanov et al, 2017). Consequently, the remaining stress-induced phosphorylation events are regulated by an unknown mechanism. We therefore tested whether and to what extent stress-induced sites that are independent of Hog1 are regulated by either PP2A^{Cdc55} or PP2A^{Rts1}. This set of sites was found to be solely affected by the deletion of CDC55 and not RTS1 (Fig 2A and B). In contrast, PP2A^{Rts1} targets a specific branch of the Hog1 signaling pathway, as we report in preprint: Hollenstein et al (2020). Thus, depending on the bound B-subunit, PP2A seems to be involved in different signaling branches during the hyperosmotic stress response. Given that PP2A^{Cdc55} is known to play a role in regulating cell cycle progression (Godfrey et al, 2017; Moyano-Rodriguez & Queralt, 2019; Touati et al, 2019), we tested whether deletion of CDC55 and our experimental stress conditions could lead to a cell cycle arrest or delayed cell cycle progression, which would indirectly result in the observed changes to the phosphorylome. We used FACS to measure DNA content profiles of the wild-type and knockout strains exposed to no stress, and 5 and 10 min of hyperosmotic stress. No significant differences in the distribution of cells could be identified (Fig EV1E). We also did not observe any particular abundance changes in well-characterized cell cycle markers covered in our dataset (Fig EV1F) (Kelliher et al, 2018). These observations refute the possibility that the increase in phosphorylation in the cdc55Δ strain can be attributed to cell cycle effects.

If PP2A^{Cdc55} activity counteracts hyperosmotic stress signaling, then stress exposure might cause inhibition of the phosphatase. The yeast Endosulfines Igo1 and Igo2 have been previously described as inhibitors of PP2A^{Cdc55} that become activated upon phosphorylation of a specific residue by the Greatwall kinase Rim15 (Juanes et al, 2013). Throughout the Rim15-Igo1/Igo2-Cdc55 regulatory module, we observed stress-induced phosphorylation events (Fig EV2A and B) and substantial phosphorylation at the respective key regulatory residues of Igo1 and Igo2 (Igo1-Ser^{64} 7.3× increase; Igo2-Ser^{63} 6× increase, Fig 2C). Phosphorylation of these residues can already be observed within seconds after hyperosmotic stress exposure, indicating a very rapid upstream sensing mechanism (Fig EV2C, Kanshin et al, 2015). Moreover, stress-induced phosphorylation of the Endosulfines appears to be transient and to return to almost basal levels after 15 min (Fig EV2D, Janschitz et al, 2019). Together these observations strongly point toward a typical stress signaling response that mediates PP2A^{Cdc55} inhibition in a very rapid and temporally regulated manner.

To test whether the Endosulfines are required for coping with hyperosmotic stress, we monitored the stress sensitivity of wild-type and igo1Δigo2Δ cells in response to high osmolarity conditions using growth curves (Fig 2D). Cells lacking IGO1/2 showed a moderate but clear susceptibility to increasing concentrations of NaCl, confirming that Igo1 and Igo2 are important for cellular survival under hyperosmotic stress conditions. Deleting CDC55 also elicited a visible growth defect at concentrations above 0.3 M NaCl, but less pronounced than with the IGO1/2 double deletion. The growth defect of igo1Δigo2Δ cells could in turn be rescued by an additional deletion of CDC55 (a triple knockout of igo1Δigo2Δcdc55Δ) under non-stressed as well as stress conditions. In fact, the growth rate of

the triple knockout was almost equivalent to the growth rate of the CDC55 single deletion, suggesting a full rescue in the monitored time period. In a similar experimental setup, we also looked at stress sensitivity to 0.8 M NaCl using a serial dilution spot assay (Fig EV2E). For both, cdc55Δ and igo1Δigo2Δ, we could confirm stress-induced growth defects.

To confirm that inhibition of PP2A^{Cdc55} is directly involved in stress signaling, we performed SILAC-MS experiments with cells exposed to hyperosmotic stress quantifying phosphorylation changes caused by the deletion of IGO1/2 (setup SR igo1Δigo2Δ) or deletion of CDC55 (setup SR cdc55Δ) (Fig 1). We observed that stress- and cdc55Δ‡-induced phosphorylation sites showed a trend toward higher phosphorylation in setup SR cdc55Δ (Figs 2E and EV2F). This was not the case in setup SR igo1Δigo2Δ. In fact, respective phosphorylation sites displayed a significant decrease in abundance. Next, we analyzed the impact of igo1Δigo2Δ in more detail, focusing on sites that were induced in cdc55Δ cells (291 sites) (Fig 2F). Nearly all cdc55Δ- and stress-induced phosphorylation sites (92%, 131 of 143 sites, 91 proteins) showed a negative fold change in setup SR igo1Δigo2Δ (Fig 2E and Set 1 and Set 2 in Fig 2F). For some of those sites, the impact of igo1Δigo2Δ was subtle, indicating that they are additionally targeted by stress-activated kinases. However, we also observed 53 phosphorylation sites (corresponding to 40 proteins) that displayed strong dependency on Igo1 and Igo2 during exposure to hyperosmotic stress (Set 1, light gray area in Fig 2F). The inhibition of PP2A^{Cdc55} is thus the main driving force of increased phosphorylation at these sites upon hyperosmotic stress exposure. In contrast, loss of IGO1 and IGO2 had no major effect on the Hog1-dependent stress phosphorylome (Fig EV2G). Our data thus demonstrate that one third of the stress-induced phosphorylome is under control of PP2A^{Cdc55}, making the phosphatase as impactful as Hog1 (Fig 2G). Taken together, we uncovered a phosphatase-driven signaling mechanism, acting in parallel to and independent of a well-established MAPK signaling pathway.

PP2A^{Cdc55} directly targets a broad range of proteins with stress-induced serine/threonine-proline motifs

To identify cellular processes affected by stress-induced PP2A^{Cdc55} inactivation, we performed a gene ontology (GO) analysis focusing on stress- and Cdc55-dependent phosphorylation sites that are either strongly (Set 1) or moderately (Set 2) affected by deletion of IGO1 and IGO2 (Fig 3A). GO terms enriched in Set 1 were found to be mostly associated with processes regulating gene expression, such as regulation of transcription, mRNA transport, and histone demethylation. GO terms derived from Set 2 were associated with multiple processes that have been previously attributed to stress signaling (Kanshin et al, 2015; Romanov et al, 2017; Janschitz et al, 2019) including processes related to transcription, signal transduction, vesicular transport as part of endocytosis, retrograde transport machineries, and actin cortical patch assembly.

PP2A^{Cdc55} preferentially dephosphorylates phospho-threonines in threonine-proline (TP) motifs (Agostinis et al, 1990; Cundell et al,

‡Correction added on 4 November 2021, after first online publication: A typo in cdc55Δ has been corrected.

2016; Godfrey *et al*, 2017; Kruse *et al*, 2020). To examine whether the proteins involved in those biological processes might be directly dephosphorylated by PP2A^Cdc55^, we first performed a motif enrichment analysis using MotifX (Schwartz & Gygi, 2005). We found the serine-proline (SP), threonine-proline (TP) to be significantly enriched (FDR < 1%) (Fig 3B), with ~60% of sites containing the

A Stress and *cdc55Δ* induced phosporylation sites
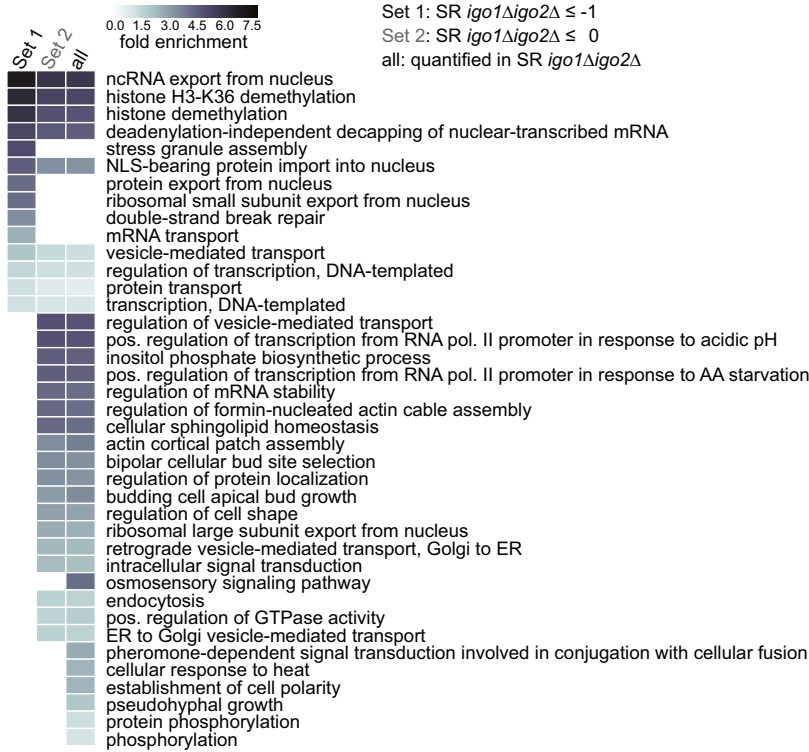
B MotifX sequence enrichment
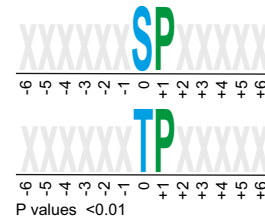
C Threonine enrichment
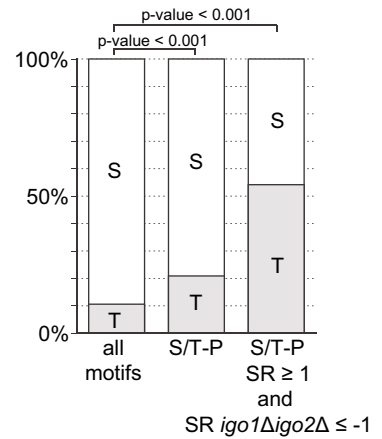
D Cdc55 M-Track assay

Figure 3.

Figure 3. Analysis of proteins affected by PP2A^Cdc55 and hyperosmotic stress.

A Gene ontology enrichment of stress- and Cdc55-dependent phosphorylation sites using DAVID v6.8 (Huang *et al*, 2009). Sets were defined according to phosphorylation site fold-changes in setup SR *igo1Δigo2Δ* (see Fig 2F). GO levels (of the category "GOTERM_BP_DIRECT") were required to be between level 3 and level 6, and GO terms should have at least two counts in the given set. The heat map illustrates the respective fold enrichments for the resulting GO terms in each set. The heat map was sorted according to the enric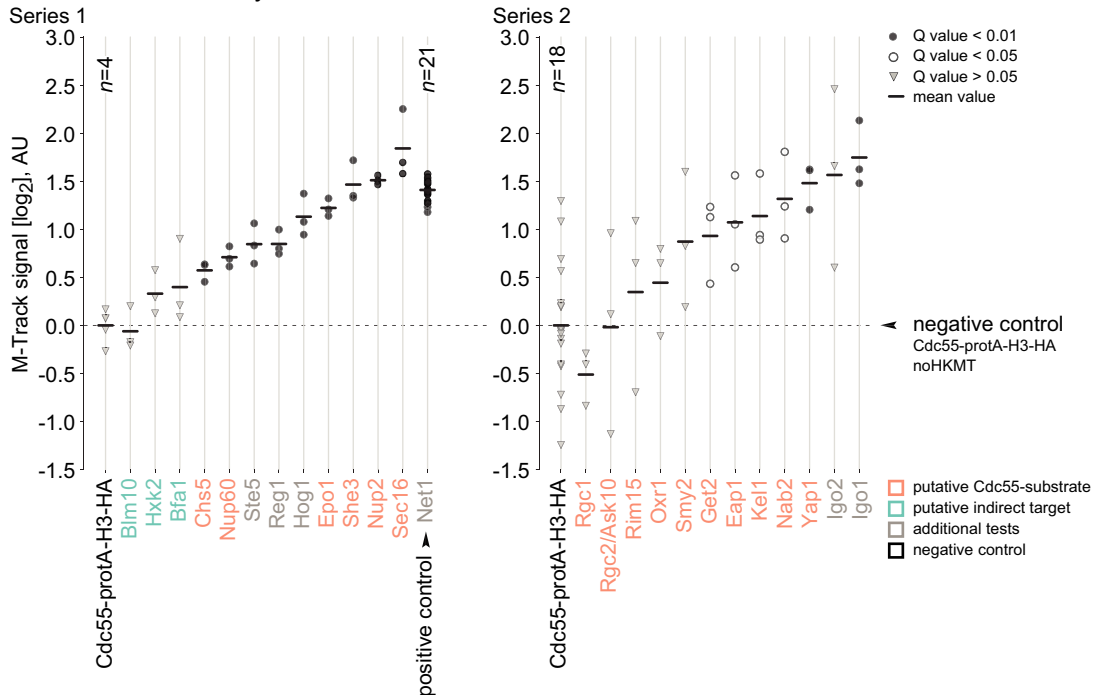hment values in Set1 and secondly according to the sum of the enrichment values in Set2 and all quantified phosphorylation sites in SR *igo1Δigo2Δ*.

B Overrepresented phosphorylation-sequence motifs calculated with MotifX. Phosphorylation sites with a fold change ≥ 2 in setup SR and ≤ 0.5 in setup SR *igo1Δigo2Δ* were compared to the whole set of phosphorylation sites quantified in setup SR and setup SR *igo1Δigo2Δ* as background.

C Bar plots illustrating the phospho-threonine enrichment of stress- and Igo1/Igo2-dependent S/T-P motifs. Phosphorylation sites quantified in both setup SR and setup SR *igo1Δigo2Δ* were analyzed. Gray bars show the percentage of phospho-threonine, white bars show the percentage of phospho-serine. The enrichment was assessed using Fisher's exact test.

D Results of the M-Track proximity assay. Cdc55 was fused to the protA-H3-HA prey-tag, and putative substrate proteins were tagged with the HKMT bait-tag. Background proximity signal was defined using a strain expressing only Cdc55-protA-H3-HA and no tagged bait protein (*negative control*) and is shown as a dashed horizontal line. Western blot signals were quantified as described in the methods section and proximity signals are displayed as log2 fold over background. Dots/triangles show signals of individual replicates ($n \geq 3$; if more than three replicates available, the sample size is indicated in the figure); horizontal bars indicate average proximity signals. Proximity signals that differ significantly from background are marked as black ($q < 0.01$) or white dots ($q < 0.05$), others as gray triangles ($q > 0.05$). AU, arbitrary units. Note that the differences in the variation and signal intensity between Series 1 and Series 2 are due to batch effects of the methylation-specific antibody used (see Methods).

motif. Moreover, the TP motif was significantly enriched within stress-induced S/T-P motifs affected by inhibition of PP2A^Cdc55 (enrichment $P < 0.001$, Fig 3C). S/T-P is the substrate motif of MAPKs and cyclin-dependent kinases (CDK). PP2A^Cdc55 counteracts global CDK phosphorylation in the context of cell cycle regulation and it has been suggested that PP2A^Cdc55 directly dephosphorylates substrates of Cdc28—the homolog of mammalian Cdk1 and the main CDK driving the cell cycle in yeast (Mendenhall & Hodge, 1998; Godfrey *et al*, 2017). To investigate whether stress- and Cdc55-dependent S/T-P sites correspond to Cdc28 substrates, we integrated our phosphoproteomic data with a published dataset analyzing the immediate impact of Cdc28 inhibition on the phosphoproteome (Kanshin *et al*, 2017) (Fig 1). The majority of S/T-P sites induced by hyperosmotic stress or deletion of *CDC55* did not display any change in abundance upon inhibition of Cdc28 (Fig EV3A and B). In detail, of the 49 stress- and Cdc55-dependent S/T-P sites, only 7 (~14%) displayed Cdc28 dependence. Vice versa, the deletion of *CDC55* also had no significant impact on S/T-P sites affected by inhibition of Cdc28 (Fig EV3B). Similar results were obtained when comparing the setup SR *igo1Δigo2Δ* with the Cdc28 inhibition data set (Fig EV3B). We also could confirm that the vast majority (> 90%) of stress- and Cdc55-dependent S/T-P sites are independent of the MAPK Hog1 (Fig EV3C). These data demonstrate that PP2A^Cdc55 targets a unique set of mainly Cdk1 independent phosphorylation sites as part of the hyperosmotic stress response. Moreover, inhibition of PP2A^Cdc55 appears to strongly regulate one third and affect more than half of all stress-induced S/T-P motifs, in contrast to Hog1, which targets about 11% of these motifs (Dataset EV1).

We next analyzed the ability of Cdc55 to interact with putative substrates *in vivo* using the M-Track protein–protein proximity assay (Zuzuarregui *et al*, 2012; Romanov *et al*, 2017). Cdc55 was tagged with the M-Track prey sequence consisting of the histone H3-hemagglutinin (HA) tag fused to protein A (protA-H3). Potential interactor proteins were fused to the enzymatic domain of the murine histone lysine methyltransferase SUV39 (HKMT-myc) serving as bait. Upon close proximity of expressed bait- and prey-protein, the protA-H3 tag becomes permanently tri-methylated on lysine 9 of histone H3 (me3K9H3). Out of 149 potential substrates of the phosphatase harboring *cdc55Δ*‡- and stress-induced S/T-P phosphorylation sites, we selected a representative group of 16 proteins

that appear in different cellular processes (Dataset EV1). Net1, the core subunit of the RENT complex, represents a well-established substrate of PP2A^Cdc55 and therefore served as a positive control (Zuzuarregui *et al*, 2012). We additionally included Igo1, Igo2, Ste5, the MAPK Hog1, and Reg1, a regulatory subunit of the protein phosphatase 1 complex, to probe for potential cross-talk with different stress signaling networks. We also included three putative indirect targets (Bfa1, Blm10, and Hxk2) that contain phosphorylation sites affected by deletion of *CDC55* but lack stress-induced S/T-P motifs. Sixteen out of 25 tested bait proteins showed a significant proximity signal (*q*-value < 0.05), including 11 out of the 16 putative substrate proteins containing Cdc55-stress-induced S/T-P motifs (Fig 3D, Appendix Fig S2A and B). These results strongly suggest that PP2A^Cdc55 not only regulates a substantial part of the stress-induced phosphorylome but also directly targets a diverse set of stress-associated proteins.

Inhibition of PP2A^Cdc55 by Igo1 and Igo2 is required for an efficient transcriptional response to hyperosmotic stress

We next focused on the role of PP2A^Cdc55 in the transcriptional regulation in response to hyperosmotic stress. Previously we observed a reduced transcriptional response to hyperosmotic stress in *cdc55Δ* cells (Reiter *et al*, 2013), which is in contrast to the finding that inhibition of PP2A^Cdc55 is part of the stress response. To avoid possible adaptation effects caused by permanent loss of PP2A^Cdc55 activity, we utilized the iAID (improved Auxin-inducible degron) (Tanaka *et al*, 2015) system to set up a conditional Cdc55 depletion system (Fig 4A). Cdc55 was readily and efficiently depleted within 30 min after induction (Fig 4B) without having any visible impact on the activation loop phosphorylation and hence activity of Hog1 upon hyperosmotic stress (Fig EV4A). Using the Cdc55-iAID strain, we performed SILAC-MS experiments to capture the immediate effect of Cdc55 depletion on the phosphoproteome. Similar to setup *cdc55Δ*, we found increased phosphorylation for several known hallmarks (Gis1, Net1, Ndd1, Sic1, Sli15, and Swe1) (Dataset EV1). In general, transient Cdc55 depletion appears to have a similar impact on the global phosphoproteome as a deletion of *CDC55*, although discrepancies between the two experimental conditions were indeed apparent (Fig 4C). Importantly, when focusing on stress-induced

phosphorylation sites, we observed an agreement of $R \sim 0.57$ between the two datasets, which is relatively high given that the steady state of a constitutive knockout is compared to a dynamic depletion after 30 min (Fig 4C). Notably, the depletion of Cdc55 did not elicit any significant cell cycle effects under the experimental conditions used (Fig EV1E). These results demonstrate that Cdc55 depletion effectively recapitulates the loss of PP2A^{Cdc55} phosphatase

activity while avoiding alterations in cellular physiology that might be caused by persistent loss of CDC55.

To test the direct effect of PP2A^{Cdc55} deprivation on transcription, we monitored the expression of two paradigm environmental stress response (ESR) genes, CTT1 (Marchler et al, 1993) and PGM2 (François & Parrou, 2001) in the Cdc55 depletion system. These ESR genes are typical and representative readouts for the transcriptional
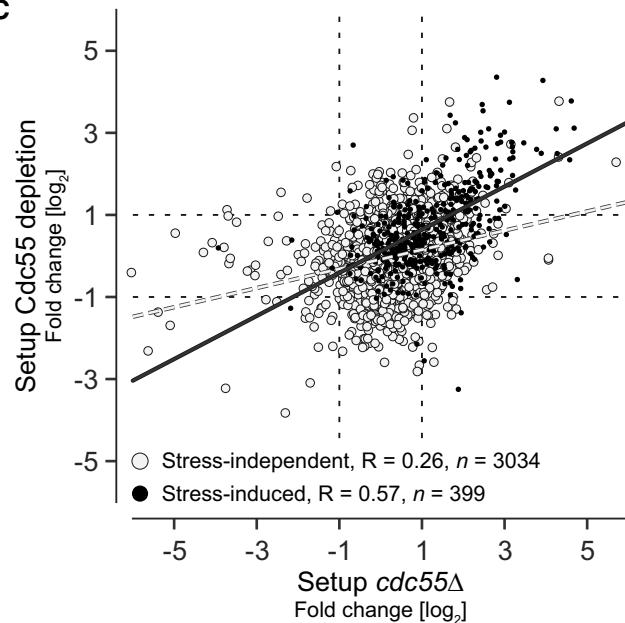

Figure 4.

◄

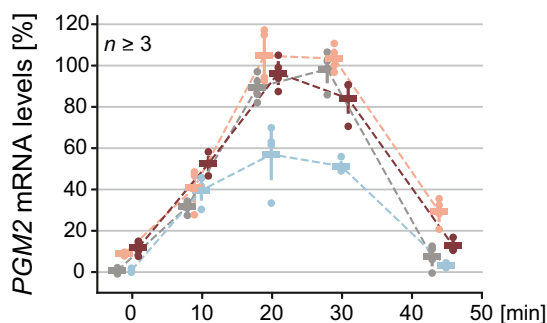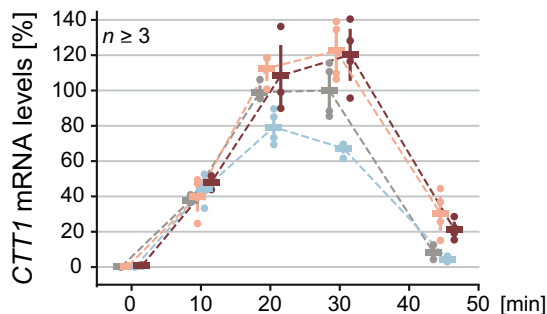response upon stress induction due to their high dynamic range (Belazzi *et al*, 1991; Rep *et al*, 1999; Gasch *et al*, 2000; Klopf *et al*, 2009; Reiter *et al*, 2013). We first recorded stress-induced transcriptional profiles for effects of Cdc55 depletion and Igo1/Igo2 deletion (Fig 4D) and observed the biggest effect of the knockouts on mRNA levels at 30 min after induction. We therefore re-measured this particular time point in a separate series of experiments (Fig 4E). Cdc55 depletion elicited no decrease but even a slightly elevated transcriptional response of both genes. In contrast, when *IGO1* and *IGO2* were deleted, we observed a strongly reduced induction of mRNA levels (Fig 4E). Cdc55 depletion rescued stress-induced transcription of *CTT1* and *PGM2* in *igo1Δigo2Δ* cells, resembling wild-type levels. Interestingly, Cdc55 depletion without stress induces a transient minor boost in transcription (˜10- and 5-fold induction of *CTT1* and *PGM2*, respectively, compared to a 700- and 40-fold induction observed after 30 min 0.5 M NaCl treatment) (Fig EV4B). These results demonstrate that PP2A^Cdc55 activity negatively affects stress-induced transcription and that inhibition of the phosphatase is required to elicit a strong transcriptional response.

PP2A^Cdc55 signaling directly regulates the transcriptional activity of Gis1 and Rph1

To understand how PP2A^Cdc55 regulates transcription in detail, we screened setups SR and SR *igo1Δigo2Δ* for transcriptional regulators with altered phosphorylation patterns (Fig 5A). The paralogous demethylase domain-containing transcriptional regulators, Gis1 and Rph1, stood out as 52–60% of their covered phosphorylation sites were found to be affected under both experimental conditions (*P* < 0.01, *t*-test relative to background). Phosphorylation of Gis1 and Rph1 has been reported to play an important role in the regulation of their transcriptional activity (Liang *et al*, 2013). In addition, Gis1 has been biochemically shown to interact with Cdc55 (Bontron *et al*, 2013).

To test for *in vivo* interaction of PP2A^Cdc55 with Gis1 and Rph1, we performed M-track assays. We used *rim15Δ* cells to prevent activation of Igo1 and Igo2 and thereby increase PP2A^Cdc55 activity, and expressed Cdc55 as prey and the transcription factors as bait proteins. Gis1 and Rph1 showed proximity signals above background control levels (Fig 5B), suggesting that the active phosphatase directly interacts with Gis1 and Rph1.

To address whether PP2A regulates stress-induced phosphorylation of Gis1 and Rph1, we examined phosphorylation-induced mobility shifts upon hyperosmotic stress in a time-resolved manner in wild-type, *igo1Δigo2Δ*-, and Cdc55-depleted cells (Figs 5C and

EV4C). In the wild type, both proteins showed a transient phosphorylation-induced upshift, peaking at around 20 min after stress induction and returning to the basal state within 45 min. When Cdc55 was depleted prior to stress induction, Gis1-HA as well as Rph1-HA exhibited increased upshifts and remained so throughout the monitored time period, indicating that PP2A^Cdc55 activity is dispensable for induction of phosphorylation but required for dephosphorylation of the proteins after termination of the stress response. Deletion of the PP2A^Cdc55 inhibitors *IGO1* and *IGO2* almost completely abolished stress-induced upshifts of Gis1 and Rph1; however, additional depletion of Cdc55 was able to fully restore the phosphorylation shifts (Fig 5C). We made similar observations for *rim15Δ* cells, which is consistent with Rim15 being the upstream activator of Igo1 and Igo2 (Fig EV5A and B). These results demonstrate that PP2A^Cdc55 needs to be inactivated to allow stress-induced phosphorylation of Gis1 and Rph1.

We next tested whether Cdc55 depletion was able to induce mobility shifts in the absence of hyperosmotic stress. Indeed, depletion of Cdc55 was sufficient to induce a rapid and time-dependent increase of Gis1 and Rph1 phosphorylation under non-stress conditions (Figs 5D and EV5C). Together with the observation that Cdc55 directly interacts with Gis1 and Rph1, this strongly suggests that inhibition of PP2A^Cdc55 in response to hyperosmotic stress shifts the balance of basal kinase and phosphatase activity affecting on Gis1 and Rph1 toward increased phosphorylation, without requiring the concurrent activation of a kinase.

Consequently, we expected alanine substitutions of stress- and Cdc55-dependent phosphorylation sites of Gis1 and Rph1 to prevent their activation and result in a reduced transcriptional response upon hyperosmotic conditions. We therefore aimed for a set of point mutations in the transcription factors to selectively inactivate stress signaling mediated by PP2A^Cdc55. To deconvolute which phosphorylation sites of the two transcription factors are affected by PP2A^Cdc55 as well as hyperosmotic stress, we captured changes in the phosphorylation pattern of Gis1 and Rph1 upon 15, 30, and 60 min depletion of Cdc55 using SILAC-MS and integrated this dataset with our phospho-proteomics datasets (Dataset EV2). Thereby, we generated detailed phospho-maps for Gis1 and Rph1, highlighting which sites are affected by PP2A^Cdc55 inhibition during the stress response. We selected a total of five S/T-P sites that were conserved between the two paralogues and displayed stoichiometric phosphorylation upon depletion of Cdc55, to be mutated to alanine (Fig 5E). Using Western blot phosphorylation shift assays, we confirmed that both point-mutated proteins become less phosphorylated upon stress exposure (Fig 5E). The remaining marginal upshift of Rph1 and

Gis1 indicates that our mutations did not cover all stress-induced sites, which was expected, since both proteins contain a multitude of non-mutated phosphorylation sites.

We next tested the effect of the alanine substitutions on the transcriptional response, using a gis1Δrph1Δ strain expressing the respective wild-type or point-mutated version of one of the proteins from plasmid. We recorded the transcriptional profiles of CTT1 and PGM2 during a period of 45 min exposure to hyperosmotic stress (Fig EV5D). While the initial increase of mRNA levels was not affected by the absence of both transcription factors, we observed a premature decline after 30 min post-stress exposure. These results suggest that Gis1 and Rph1 do not function during the early induction of the transcriptional stress response but rather support a high transcriptional output over an extended period of time. Since we observed the strongest effect after 30 min exposure to hyperosmotic stress, we re-measured this time point in a separate experiment and observed the mRNA levels of CTT1 and PGM2 decrease by 50–100% for the 5A mutant alleles relative to the respective knock out (Fig 5F). We therefore propose that direct dephosphorylation by PP2A^{Cdc55} suppresses the transcriptional activity of Gis1 and Rph1 and that hyperosmotic stress-mediated inhibition of the phosphatase is necessary to allow phosphorylation-induced activation of these transcription factors.

In summary, our results portray PP2A^{Cdc55} as a central downstream effector of a phosphatase-centric signaling pathway, which causes major phospho-proteomic changes and thereby enables cellular adaptation in response to extracellular stimulation.

Discussion

Reversible protein phosphorylation is widely studied to understand cellular behavior; however, the regulatory underpinning of phospho-proteomic adaptations is still largely unknown. Historically, research to understand the phosphorylome has mainly focused on kinase signaling pathways, while the possible active contribution of phosphatases has not received similar attention. Here, we propose a signaling principle, in which the inhibition of a phosphatase is the key event resulting in increased phosphorylation, while induction of kinases affecting the same substrates appears not to be required.

PP2A^{Cdc55} stands at the core of a signaling pathway that is required and sufficient to induce phosphorylation of a wide range of proteins as part of the hyperosmotic stress response in budding yeast. The majority of the PP2A-affected phosphorylation sites correspond to S/T-P motifs. Absence of the phosphatase activity is required for the stress-induced phosphorylation of these sites. Moreover, depletion of Cdc55 under unstressed conditions is sufficient to induce a similar phosphorylation response. Thus, regulation of PP2A activity constitutes the main driving force behind these particular phosphorylation changes. From a classical kinase-centric point of view, one expects PP2A^{Cdc55} to control a downstream kinase that mediates those phosphorylations, rather than directly acting on a broad set of substrates (Chan & Amon, 2009; Park et al, 2012; Khanna et al, 2013; Wandzioch et al, 2014; Courtney & Deiters, 2019). S/T-P motifs, for that matter, are targeted by CDKs and MAPKs. It is also well known that PP2A^{Cdc55} antagonizes Cdk1 phosphorylation during the cell cycle (Mochida et al, 2009; Godfrey et al, 2017; Touati et al, 2019). However, we find that inhibition of Cdc28 does not affect stress-induced S/T-P phosphorylation sites and that PP2A^{Cdc55} acts on a complementary set of S/T-P sites during hyperosmotic stress (Fig EV3A and B). Interestingly, the CDK Pho85 has been described to mediate hyperosmotic stress signaling, but appears to be located upstream of Rim15, and therefore also of PP2A^{Cdc55} (Wanke et al, 2005; Jin et al, 2017). The other CDKs in yeast have been primarily connected to transcription-related phosphorylation events (Nishizawa et al, 2010) and would therefore not account for the majority of targeted substrates. There is also evidence that none of the five proline-directed MAP kinases in S. cerevisiae could act as the hypothetical stress-activated counter-kinase downstream of PP2A^{Cdc55}. The MAPK Smk1 is not expressed in haploid cells, and the MAPKs Slt2 and Fus3 do not become activated during the immediate stress response (Pierce et al, 1998; García-Rodríguez et al, 2005; Hao et al, 2008). We found over 90% of stress- and PP2A^{Cdc55}-dependent S/T-P motifs to be independent of Hog1, while deletion of the MAPK Kss1 has been described to not affect Hog1-independent, stress-induced S/T-P sites (Romanov et al, 2017). Thus, none of the proline-directed kinases appear to act downstream of PP2A^{Cdc55}. Moreover, our experiments imply that the phosphatase directly targets these S/T-P phosphorylation sites, pointing toward a phosphatase-centric signaling mechanism as depicted in Fig 6. Based on our results, we propose the following

Figure 5. Transcriptional activity of Gis1 and Rph1 is activated by inhibition of PP2A^{Cdc55}.

A   Venn diagram of 14 transcription factors [as recovered from the YEASTRACT database (Teixeira et al, 2006, 2018)] with at least one phosphorylation site changing twofold in setup SR (gray) or SR igo1Δigo2Δ (blue). For the six overlapping transcription factors, the log2 SILAC ratios of phosphorylation sites are shown (y-axis) in the corresponding setups (color code as above). The first two box plots illustrate the distribution of log2 SILAC ratios of all phosphorylation sites quantified in each setup ('all'). Gis1 and Rph1 were found to be significantly different in their distributions (P < 0.01, t-test relative to "all").

B   M-Track proximity assay of Cdc55 fused to the protA-H3-HA prey-tag and Gis1, respectively, Rph1, tagged with the HKMT bait-tag expressed in a rim15Δ strain background. Background signal intensity was defined using a strain expressing only Cdc55-protA-H3-HA and no tagged bait protein (noHKMT). Positive control: Nup2-HKMT, CDC55-protA-H3HA. me3: antibody recognizing me3K9H3; HA: 12CA5 antibody.

C   Mobility shift assays monitoring phosphorylation-induced mobility changes of Gis1 (two upper rows) and Rph1 (two lower rows) upon hyperosmotic stress in wild-type, igo1Δigo2Δ-, and Cdc55-depleted cells (right-hand side).

D   Mobility shift assay of Gis1 and Rph1 across several time points after Cdc55 depletion (without exposure to hyperosmotic stress). Cdc28: loading control (shown in Fig EV5C).

E   Western blot phosphorylation shift assays of wild-type Gis1-myc (upper panel) and Rph1-Flag (lower panel), and mutated forms Gis1-5A-myc (upper panel) and Rph1-5A-Flag (lower panel). The measurement was done using Phos-tag (Kinoshita et al, 2006) and at the indicated time points after exposure to hyperosmotic stress (0.5 M NaCl) using Pgk1 protein levels as a negative control. The location of the mutated residues is shown in the respective schematics. Red boxes: demethylase associated domains (JmjN and JmjC), blue box: zinc finger domain.

F   Transcriptional analysis of stress-induced expression of ESR genes CTT1 (upper panel) and PGM2 (lower panel) at 30 min post-stress across indicated strains expressing either wild-type or point-mutated forms of Gis1 and Rph1 in a gis1Δrph1Δ deletion background, with the empty vector as control.

A
Transcription Factors

B
Protein-protein proximity

rim15Δ
Cdc55-protA-H3-HA

C
Cdc55 depletion system

D
Cdc55 depletion system

E

F
W303-1A *gis1Δrph1Δ*
+ 0.5 M NaCl, 30 mins
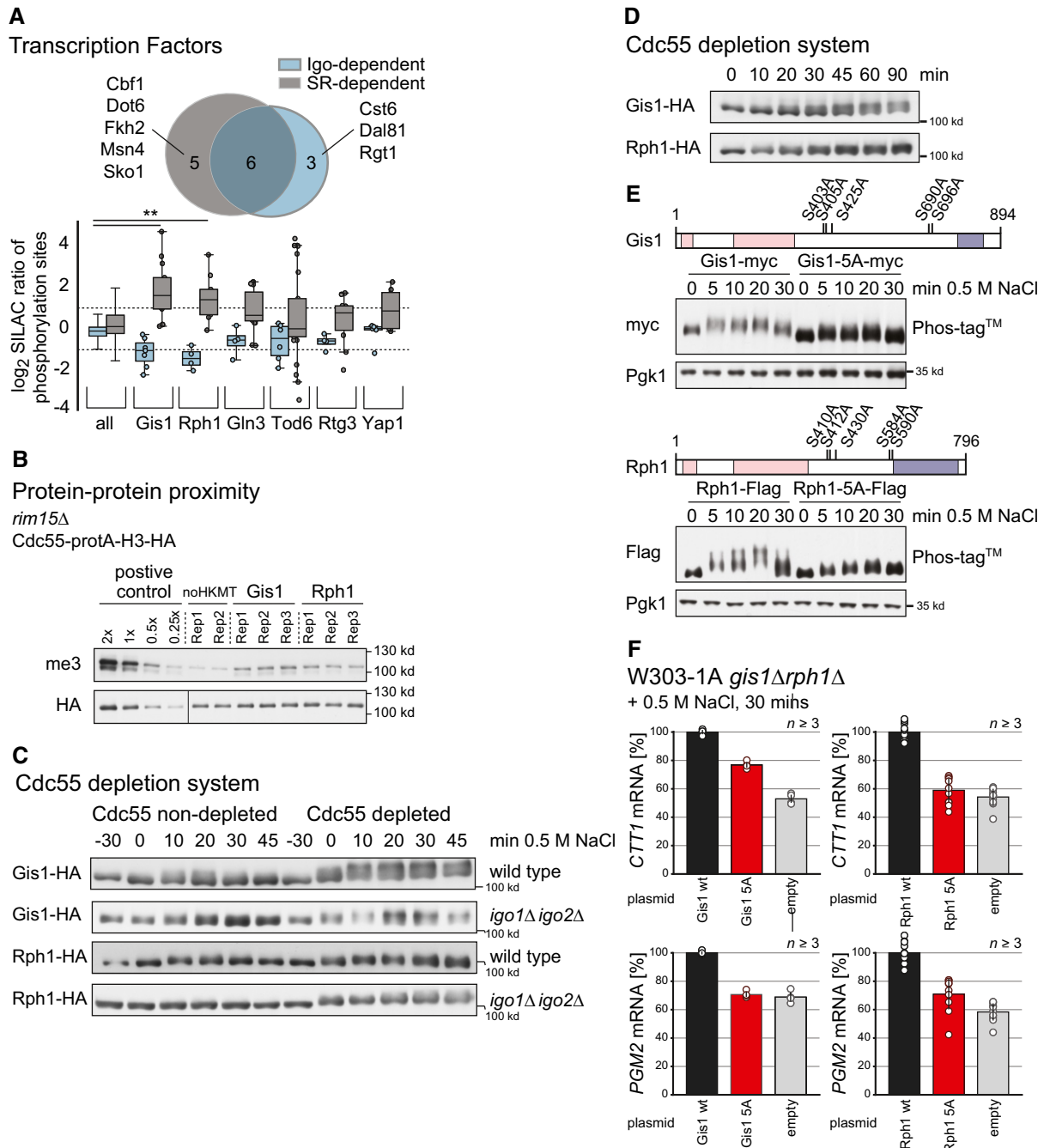
Figure 5.

model: Under unstressed conditions, the phosphatase and counteracting kinase activities are balanced, resulting in a steady state of low phosphorylation of shared substrates. Upon hyperosmotic stress, the phosphatase becomes inhibited, tipping the balance toward increased net phosphorylation, rendering it a key event in regulating a global signaling response. In fact, our detailed analysis of the phosphorylation behavior of the Cdc55 substrates Gis1 and Rph1 further substantiates the proposed model. In an alternative scenario, PP2A^{Cdc55} could inhibit the activity of one or several unknown kinases under non-stress conditions that share common S/T-P substrate sites with the phosphatase. Inhibition of PP2A^{Cdc55}

would result in activation of these kinases and therefore an increase in phosphorylation due to the combinatory effects of phosphatase inhibition and simultaneous kinase activation. However, as described in detail before, there is no evidence that the shift in the balance of substrate phosphorylation is associated with the activation of any known proline-directed kinase. Further studies will undoubtedly be required though to conclusively prove that no concurrent kinase activation takes place upon PP2A^{Cdc55} inhibition. Stress-induced inhibition of PP2A^{Cdc55} works through the Greatwall Kinase-Endosulfine module, constituting a conserved three-tiered signaling pathway with the phosphatase as the core element
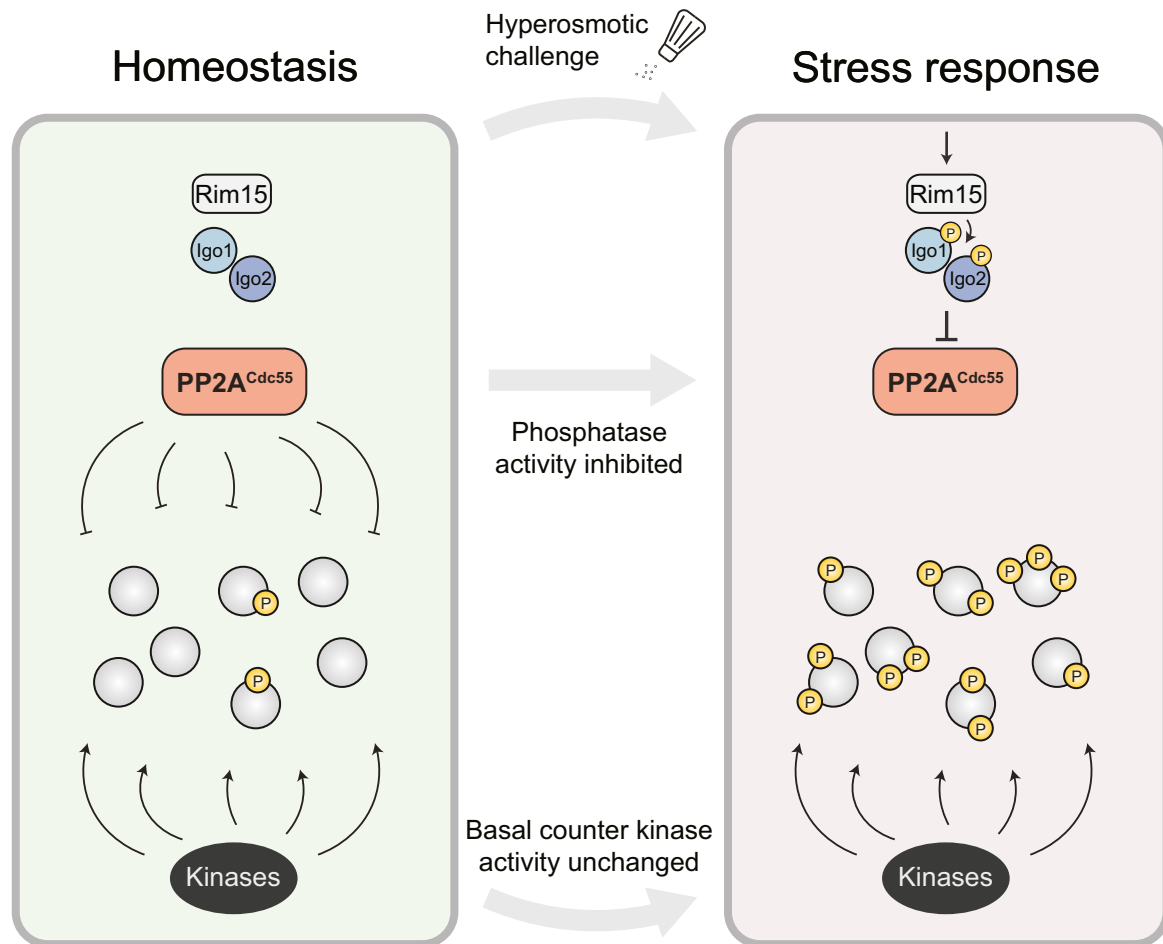
Figure 6. PP2A^Cdc55 pathway.

The phosphatase PP2A^Cdc55 lies at the center of a hyperosmotic stress signaling cascade. Under non-stress conditions (left), the balanced activities of PP2A^Cdc55 and counteracting kinase(s) result in a steady state of low phosphorylation of shared substrates. Hyperosmotic stress signaling transmitted through the Greatwall kinase/ Endosulfine module activates the PP2A^Cdc55 inhibitors Igo1 and Igo2 via phosphorylation at key regulatory sites (right). The resulting inhibition of the phosphatase is essential to tip the balance toward increased net phosphorylation.

(Mochida & Hunt, 2012; Castro & Lorca, 2018). This pathway has been described to function in the context of cell cycle regulation and nutrient starvation, where it assists the increased activity of a kinase by inhibition of the counteracting phosphatase PP2A^Cdc55 (Juanes *et al*, 2013; Sarkar *et al*, 2014), but never as a stand-alone effector system without simultaneous kinase activation. Inhibition of PP2A^Cdc55, as the main downstream signaling effector, causes major phosphorylation changes upon hyperosmotic stress to elicit a transcriptional response allowing for cellular adaptation. The signaling is terminated once the phosphatase becomes activated again, restoring the pre-stressed state of the phosphorylome (Williams *et al*, 2014). The discovery of this phosphatase-centric signaling mechanism is surprising since it represents the exact opposite to the traditional view of the rather passive role of phosphatases as antagonists of kinase-mediated signaling.

The mammalian version of PP2A plays a key role in the pathogenesis of various human diseases, ranging from cancer and neurodegenerative diseases to immunoregulatory dysfunctions (Perrotti & Neviani, 2008; Sontag & Sontag, 2014; Apostolidis *et al*, 2016; Meeusen & Janssens, 2018; Westermarck, 2018; Bao *et al*,

2020). It is due to PP2A's systemic impact on cellular processes that it is highly relevant to precisely understand its action and regulation (Westermarck, 2018). Given that all elements of the Greatwall Kinase-Endosulfine-PP2A-B55 pathway are highly conserved, it is not unlikely that a similar PP2A-B55-driven signaling response exists in mammalian cells. Looking at PP2A as an active and broadly acting downstream signaling effector in addition to its role as an antagonist of kinases could therefore potentially assist approaches in tackling human diseases (Álvarez-Fernández *et al*, 2018; Kauko *et al*, 2018; McClinch *et al*, 2018; O'Connor *et al*, 2018; Mazhar *et al*, 2019).

Our description of such a phosphatase-driven signaling response leads to the question as to whether this mode of action applies to other phosphatases. There are two other prominent phosphatase-centric pathways where the phosphatase represents a regulated effector element that directly targets a broad set of substrates, PP2B and PP1. PP2B has been mainly described to become activated by increased intracellular Ca^{2+} levels, which results in dephosphorylation of PP2B substrates (Park *et al*, 2019; Creamer, 2020). This is distinctly different from our proposed model, where the basal

activity of the phosphatase becomes inhibited causing the exact opposite impact on the phosphorylome. PKA signaling, on the other hand, seems to follow a similar architecture as we describe here with the inhibition of PP1 leading to increased phosphorylation for example in neurons (Leslie & Nairn, 2019). This seems to primarily affect PKA substrates, which appear to require both activation of PKA and inhibition of PP1. It is likely that inhibition of PP1 could be sufficient to induce phosphorylation of non-PKA substrates as well and thus could represent a similar modus operandi as we describe for PP2A^{Cdc55} in the context of stress signaling. Such mechanistic details and their systematic dissection still remain to be explored for many phosphatases. One of the reasons that could complicate such studies might lie in the difficulty of tracking phosphatase activity and understanding the underlying complex regulatory mechanisms (Shi, 2009; Fahs *et al*, 2016). In recent years, different approaches have emerged for selective phosphatase inhibition, ranging from targeted protein degradation, inducible CRISPR tools to chemical inhibitor compounds (Köhn, 2020). These technological developments, along with the increasing throughput and accessibility to MS-based proteomics technologies, are the perfect platform to investigate the existence of other potential phosphatase-driven signaling mechanisms.

Another important factor that might have hampered the discovery of such signaling mechanisms is the natural assumption that an induction of phosphorylation upon a signal is ultimately caused by the activation of a kinase rather than the inhibition of a phosphatase. However, the regulation of positive phosphorylation in signaling responses is only partly explained by kinase signaling so far. As such, the concept of phosphatase-driven signaling mechanisms could provide an alternative explanation of how these phospho-proteomic-adaptations are achieved. Considering that in our study as much as 30% of stress-induced phosphorylation is regulated by PP2A^{Cdc55}, the impact of such phosphatase signaling could be quite significant. The extent to which phosphorylation can be fine-tuned would also be severely increased due to potential synergistic interaction between phosphatase and kinase pathways on shared substrates (García-Blanco *et al*, 2019). We therefore argue that our unexpected findings of phosphatase inhibition as a mechanism to induce a positive phosphorylation response could be pivotal for a holistic understanding of cellular signaling.

Materials and Methods

Yeast strains and plasmids

Saccharomyces cerevisiae strains used in this study are listed in Table EV2 (Thomas & Rothstein, 1989). Strains WR365 (W303-1A SILAC, *cdc55Δ*, Mat a) and WR366 (W303-1A SILAC, *cdc55Δ*, Mat α) were obtained by transforming WR209 (W303-1A SILAC, Mat a) and WR210 (W303-1A SILAC, Mat α) (Reiter *et al*, 2012) with an *CDC55* deletion cassette, amplified by PCR using corresponding S3 and S4 primers and plasmid pGA2260/pFA6a-*HIS3MX6* as template (Wach *et al*, 1994). Strain WR1739 (W303-1A SILAC, *igo1Δigo1Δ*, Mat a) was obtained by transforming WR209 with respective deletion cassettes amplified from plasmids pFA6a-*hphMX6* and pFA6a-*natMX6* (Hentges *et al*, 2005). Other deletion mutant strains were generated as follows: W303-1A was transformed with PCR

amplifications of the corresponding deletion cassettes, using plasmids pGA2260/pFA6a-*HIS3MX6* (Wach *et al*, 1994), pGA2264/pFA6a-*TRP1MX6* (Wach *et al*, 1994), pGA2259/pFA6a-*kanMX6* (Wach *et al*, 1994), pFA6a-*hphMX6* (Hentges *et al*, 2005), or pFA6a-*natMX6* (Hentges *et al*, 2005) as templates and primers designed as described above, giving rise to yeast strains GG589, GG593, GG594, JF83, JV1028. Construction of iAID strains involved multiple cloning steps: First, a n-terminal AID*-tagging cassette for *CDC55* was constructed by subcloning the AID* DNA sequence (PCR-amplified from p2352 (Morawska & Ulrich, 2013) into YIPlac211 and subsequent insertion of the tetO7-CYCmin promoter sequence and a 654bp n-terminal fragment of *CDC55* (in frame), resulting in plasmid pGG95 (YIPlac211-tetO7-CYCmin-AID*-N-*CDC55*). Yeast strains W303-1A and WR209 were transformed with restriction cut pL235 (PTA4998™; ATCC) for integration of *Oryza sativa* TIR1 (OsTIR1) gene into the *HIS3* locus. Positive transformants were transformed with PCR products encoding the tetO7-CYCmin-AID*-N-*CDC55* cassette amplified from pGG95. tTA (tetR-VP16) was subcloned into pL253 (replacing OsTIR1), resulting in a *GPD1*-promoter-tTA fusion that was introduced into YIPlac128, giving rise to pGG92 (YIPlac128-pGPD1-tTA). The tTA-containing fragment was amplified by PCR and integrated into the *LEU2* ORF, resulting in yeast strains GG163 and GG292. Deletion mutant derivatives of GG163 (Table EV2) were constructed as described above. Endogenous tagging of *GIS1* and *RPH1* with hemagglutinin (HA)-tags (yeast strains GG267, GG274, GG590, GG592, GG597, and GG600) was obtained by transformation of W303-1A and GG163 with HA-tagging cassettes PCR-amplified from plasmid pYM3/pGA2255/pFA6a-6HA-*kanMX6* (Knop *et al*, 1999). Endogenous tagging of *GIS1* and *RPH1* with HTBeaq (Reiter *et al*, 2012) was achieved by transformation of GG292 with HB-tagging cassettes amplified from plasmids pWR268 and pWR160 (Reiter *et al*, 2012) resulting in yeast strain GG573. Yeast strains used in M-track assays were generated as follows: WR974 (S288c *CDC55*-TEV-Protein A-Histone3-HA, Mat a) was obtained by transforming a S288c *CDC55*-GFP strain (WR968) of the yeast strain-library available from Life Technologies (http://clones.lifetechnologies.com; Huh *et al*, 2003) with PacI/SacI cut plasmid pCK902, encoding the TEV-ProteinA-Histone3-HA cassette (Brezovich *et al*, 2015). WR1030 (S288c *CDC55*-TEV-ProteinA-Histone3-HA, Mat α) was obtained from backcrossing WR1242 with a S288c wild-type, Mat α strain. M-track strains WR1111–WR1771 were obtained by transformation of corresponding GFP library strains (Huh *et al*, 2003) with PacI/PmeI restriction digests of plasmid pCK900, encoding the myc-HKMT tagging cassette. Positively tested transformants were crossed with WR1030 resulting in the final M-track strains. M-track strains MJ334 to MJ336 were obtained by transformation of WR974 with PCR amplifications of the myc-HKMT tagging cassette (Brezovich *et al*, 2015). For PCRs, plasmid pJA31 (Janschitz *et al*, 2019) and corresponding primers designed according to (Wach *et al*, 1994; Knop *et al*, 1999) were used. Yeast strains GG628 and GG630 were obtained by transformation of WR1211 and WR1485 with a *RIM15*-deletion cassette PCR-amplified from plasmid pFA6ahphMX. PCRs were performed using Q5 polymerase (NEB) according to the manufacturer protocol. All plasmids used in this study are listed in Table EV3. Manipulations of plasmid DNA were carried out using the In-Fusion® cloning kit (Takara) according to the manufacturer's guidelines. To create plasmids pJF83 (YIPlac211-9xmyc-*GIS1*) and pJF97 (YIPlac128-

6xFLAG-*RPH1*), ORF sequences of *GIS1* and *RPH1* were amplified via PCR from W303-1A genomic DNA and subcloned into variants of plasmids YIPlac211 and YIPlac128 for n-terminal tagging. Round-the-horn mutagenesis (Moore & Prevelige, 2002) was used to generate 5A mutations of *GIS1* and *RPH1* giving rise to plasmids pJF91 (YIPlac211-9xmyc-*GIS1*-5ALA) and pJF98 (YIPlac128-6xFLAG-*RPH1*-5ALA). Plasmids YIPlac211-9xmyc-*GIS1* and YIPlac128-6xFLAG-*RPH1* were used as template in PCRs. PCRs were run using Phusion HF DNA polymerase (NEB) according to the manufacturer protocol. Methylated template DNA was digested by DpnI treatment at 37°C for 60 min.

Growth conditions, SILAC labeling, and harvesting

Yeast cells were grown shaking (200 rpm) at 30°C for at least ten generations until mid-log phase ($OD_{600\,nm}$ ~1). For MS experiments, SILAC labeling (Ong *et al*, 2002; Gruhler *et al*, 2005) was performed as follows: Yeast cultures were grown in 50 ml synthetic medium (0.17% yeast nitrogen base, 0.5% ammonium sulfate, 2% glucose, amino acids as required) supplemented either with heavy- or light-labeled arginine and lysine (0.05 mg/ml of L-arginine-HCl and 0.05 mg/ml of L-lysine-2HCl, Euriso-top), harvested by filtration (Protran 0.45-μm nitrocellulose membrane, Amersham), and frozen in liquid N_2. For each experiment, heavy- and light-labeled cultures were grown in parallel and frozen pellets were united after harvesting. Details on the setup of MS experiments are provided in Table EV1. Hyperosmotic stress was induced by addition of 0.5 M NaCl (final concentration) for times indicated. Cdc55 depletion samples were treated with 0.02 mg/ml doxycycline (Sigma-Aldrich) and 1 mM Auxin (3-indoleacetic acid, Sigma-Aldrich) for 30 min prior to hyperosmotic stress application. For mock treatment, H_2O and ethanol were used, respectively. For M-Track experiments and gene expression analysis, yeast cultures were grown in 50 ml rich medium (YPD; 1% yeast extract, 2% peptone, 2% glucose), harvested by centrifugation (2×1.5 min, $3,000 \times g$), and frozen in liquid N_2. For growth rate experiments cells were grown in YPD at 30°C overnight. Cultures were adjusted to $OD_{600\,nm}$ of 0.1 and grown to $OD_{600\,nm}$ 0.8 in fresh YPD at 30°C. 20 μl of the cultures were added to each well of a 96-well flat-bottom plate (Corning Inc., Corning, United States) containing 180 μl of fresh YPD media containing different concentrations of NaCl. The final concentration of NaCl ranged from 0 M to 1.25 M as indicated. Plates were incubated at 30°C for 24 h (Cytomat 2, Thermo Fisher, Waltham, United States). Each experiment was run in triplicate on separate microplates. $OD_{600\,nm}$ was measured hourly in an automated setup (Synergy H1 reader, Biotek, Winooski, United States; Rack Runner 720, Hamilton Robotics, Martinsried, Germany).

MS study design

In the study presented here, we compare data from a number of large-scale MS-based phospho-proteomic experiments. In addition, we integrate previously published MS datasets to analyze the behavior of groups of phosphorylation sites in a variety of experimental conditions. The integration of multiple datasets leads to a high number of missing values, which is a well-known problem of data-dependent MS studies. To address this issue, we chose the following strategy to analyze the phospho-proteomic data. We first checked whether changes in protein abundance could potentially confound the quantification of the phosphoproteome. (i) In general, we observed relatively stable levels of protein abundance, suggesting no or only a minor effect on the phosphorylation site ratios (see Fig EV1B). Hence, we did not adjust phosphorylation ratios accordingly because non-phosphorylated peptide data were not available for all phosphorylation sites. (ii) Instead of filtering for quantification in multiple replicates and statistically testing individual phosphorylation sites, we statistically compared the behavior of defined groups of phosphorylation sites (e.g., stress-induced phosphorylation sites).

Protein extraction and enzymatic digestion for MS experiments

Proteins were extracted using TRIzol (Invitrogen) (Reiter *et al*, 2012), or (for setup SR *igo1Δigo2Δ*) using a TCA-based protocol. TCA extraction was performed as follows: Cells were resuspended in 8 M urea, 50 mM Tris pH 8.0 and disrupted by beat beating using a Fast Prep (three cycles: 45 s, power level 5.5). Insoluble material was removed by centrifugation. Proteins were extracted by addition of ice-cold TCA (15% final concentration), followed by an incubation for 60 min on ice. Proteins were centrifuged ($12,000 \times g$, 5 min, 4°C), washed in 15% TCA and acetone, and shortly dried. Protein pellets were resuspended in 50 mM ammonium bicarbonate (ABC) buffer containing 8 M urea. Protein concentration (2–3 mg/ml) was determined by Bradford protein assay (Bio-Rad), using bovine serum albumin to create a standard curve. Protein samples were diluted to 50 mM ABC, 6 M urea by using 50 mM ABC. Disulfide bridges were reduced by adding dithiothreitol (DTT), using a DTT to protein ratio of 1:50 (w/w), and samples were incubated for 30 min at 56°C. Cysteines were alkylated by adding iodoacetamide (IAA), using an IAA to protein ratio of 1:10 (w/w), and samples were incubated for 30 min in the dark at room temperature. Remaining IAA was quenched by adding DTT, using a DTT to protein ratio of 1:100 (w/w). Proteins were digested with LysC (Roche) for 2 h at 30°C, using a LysC to protein ratio of 1:100 (w/w). Protein samples were diluted to 50 mM ABC 0.6 M urea by using 50 mM ABC. Proteins were digested with trypsin (Trypsin Gold, Promega) overnight at 37°C, using a trypsin to protein ratio of 1:60. The overnight digest was stopped by adding 100% trifluoroacetic acid (TFA) to a final concentration of 1%. Resulting peptide samples were desalted using Strata-X reversed-phase polymeric solid-phase extraction cartridges Phenomenex, 200 mg) and eluted by addition of 70% acetonitrile (ACN) 0.1% formic acid (FA). An aliquot of ~1 μg protein extract was taken, diluted with 0.1% TFA to an ACN concentration below 2%, and subjected to MS analysis. Peptide samples were snap-frozen in liquid nitrogen, lyophilized, and stored at −80°C.

Phosphopeptide isolation and fractionation

Phosphopeptides were enriched using TiO_2 (Titansphere bulk media, 5 μm, GL Science). The amount of TiO_2 resin was adjusted to the peptide concentration (1.25 mg of TiO_2 / 3.5 mg yeast protein extract). TiO_2 resin was washed with 50% methanol, H_2O and equilibrated with TiO_2 loading buffer (0.8 M phthalic acid, 80% ACN, 0.1% TFA). Dried peptide samples were dissolved in 100 μl TiO_2 loading buffer and incubated for 1 h with 1 mg TiO_2 resin per 2.8 mg protein extract. The TiO_2 resin was transferred to a Mobicol spin column and washed with 2×250 μl TiO_2 loading buffer,

2 × 250 µl 80% ACN 0.1% TFA, 2 × 250 µl 1% ACN 0.1% TFA. Bound phosphopeptides were eluted by addition of 2 × 150 µl 0.3 M ammonium hydroxide and acidified to pH 2.5 by addition of 10% TFA. Phosphopeptide samples were desalted using C18 Sep-Pak cartridges (Waters), vacuum-dried, and stored at −80°C. Phosphopeptides were fractionated offline by strong cation exchange chromatography (SCX), using 1 ml Resource S column (GE healthcare) installed in a nano-HPLC machine (Ultimate 3000, Thermo Fisher Scientific). Briefly, samples were injected using SCX Buffer A (5 mM NaH$_2$PO$_4$, 30% acetonitrile (ACN), pH 2.7). Peptides bound to the column were separated by a linear gradient of sodium chloride in SCX buffer A. Based upon UV measurements, some fraction containing low amounts of peptide were pooled which resulted in a total of 12 fractions (fractions were collected every minute and then pooled together). Each elution sample was adjusted by TFA to pH 2–3 for subsequent desalting (Rappsilber *et al*, 2007) and mass spectrometry measurement.

Poly-histidine, biotinylation signal tandem affinity (HB) purifications

For HB pull-downs, one liter of yeast cell culture was harvested by filtration, deep-frozen, and ground using a SPEX Freezer Mill 6870 (SPEX SamplePrep) applying standard settings (Reiter *et al*, 2012). Lysed cells were resolved in buffer 1 (6 M guanidine HCl, 50 mM Tris pH 8.0, 5 mM NaF, 1 mM PMSF, 2 mM sodium orthovanadate 0.1% Tween, protease inhibitor cocktail (Roche), pH 8), cleared by centrifugation (13,500 × *g*, 15 min, 4 °C), incubated with Ni^{2+}−Sepharose beads (GE Healthcare) for 4 h at room temperature, and washed with urea buffer (8 M urea, 50 mM sodium phosphate buffer pH 8.0 (and pH 6.3), 300 mM NaCl, 0.01% Tween 20). Proteins were eluted in urea buffer pH 4.3 containing 10 mM EDTA, incubated with streptavidin–agarose beads (Thermo Fisher Scientific), washed with urea wash buffer containing 1% SDS and without SDS. For on bead digests, samples were re-buffered to 50 mM ammonium bicarbonate (ABC), reduced using DTT, treated with 20 mM iodoacetamide (IAA) to alkylate cysteine residues, incubated with 300 ng trypsin (Trypsin Gold, Mass Spectrometry Grade, Promega) at 37 °C overnight, quenched with trifluoroacetic acid (0.5% final concentration), and desalted using C18 StageTips (Rappsilber *et al*, 2007).

Mass spectrometry measurements

LC-MS/MS analysis was performed on an UltiMate 3000 Dual LC nano-HPLC System (Dionex, Thermo Fisher Scientific), containing both a trapping column for peptide concentration (PepMap C18, 5 × 0.3 mm, 5 µm particle size) and an analytical column (PepMap C18, 500 × 0.075 µm, 2 µm particle size, Thermo Fisher Scientific), coupled to a Linear Trap Quadrupole Orbitrap Velos (with CID, collision-induced dissociation mode; or ETD, electron-transfer dissociation) mass spectrometer (Thermo Fisher), a Q Exactive HF Orbitrap (with HCD, higher-energy collisional dissociation mode) mass spectrometer (Thermo Fisher), or a Orbitrap Lumos Tribrid (with HCD) mass spectrometer (Thermo Fisher) via a Proxeon nanospray flex ion source (Thermo Fisher). For peptide separation on the HPLC, the concentration of organic solvent (acetonitrile) was increased from 2.5 to 40% in 0.1% formic acid at a flow rate of 275 nl/min, using different gradient times. For acquisition of MS2 spectra, the instruments were operated in a data-dependent mode with dynamic exclusion enabled. A detailed description of the acquisition settings for individual raw files is listed in Dataset EV3.

HB purifications were analyzed on a Q Exactive HF Orbitrap (Thermo Fisher Scientific) mass spectrometer applying the following settings: Peptides were separated applying an increasing organic solvent (acetonitrile) gradient from 2.5 to 40% in 0.1% formic acid over 120 min at a flow rate of 275 nl/min. MS1 resolution was set to 120 k, AGC 3E6. MS2 resolution was set to 30 k, AGC 1E5, 250 ms max. IIT. The mass spectrometer was configured to pick the eight most intense precursor ions for data-dependent MS2 scans, applying HCD for fragmentation with a normalized collision energy (NCE) of 27. Dynamic exclusion time was set to 30 s.

Mass spectrometry raw data files used in this study

MS raw files and MS data analysis results from this study have been deposited to the ProteomeXchange Consortium (Vizcaíno *et al*, 2016) via the PRIDE partner repository with the dataset identifier PXD019646. Previously published MS raw files from Romanov *et al* (2017) that were reanalyzed in this study are available in the PRIDE repository with the dataset identifiers: PXD004294 to PXD004300 (Data ref: Romanov *et al*, 2017).

Mass spectrometry data analysis with MaxQuant

Raw MS data were analyzed using MaxQuant (Cox & Mann, 2008) software version 1.5.2.8 (global proteome experiments) or with version 1.6.0.16 (Gis1 and Rph1 HB purification experiments), using default parameters with the following modifications. MS2 spectra were searched against a protein database from the SGD (Saccharomyces Genome Database, www.yeastgenome.org, version 3$^{\text{rd}}$ February 2011) containing 6,717 entries, concatenated with a database of common laboratory contaminants (provided with MaxQuant). Hence, the option to include contaminants was deactivated. Enzyme specificity was set to "Trypsin/P" (allowing cleavage after proline), the minimal peptide length was set to 6 and the maximum number of missed cleavages was set to 2. The option "I = L" was activated to treat the amino acids leucine and isoleucine as indistinguishable. The minimum peptide length was set to 6. Carbamidomethylation of cysteine was defined as fixed modification. "Acetyl (Protein N-term)", "Deamidation (NQ)", "Oxidation (M)" and "Phospho (STY)" were set as variable modifications. A maximum of 6 variable modifications per peptide was allowed. For MS measurements of samples prior to phosphopeptide enrichment "Phospho (STY)" was not used as a variable modification. For SILAC quantification, "multiplicity" was set to 2, "Arg6" and "Lys6" were specified as heavy labels, "Requantify" and "Match between runs" were enabled.

Calculation of phosphorylation site SILAC ratios

For calculation and normalization of phosphorylation site, SILAC ratios in-house Python scripts were used (see Data and Code Availability section). All data were extracted from MaxQuant evidence tables. SILAC ratios (heavy to light) were extracted from the column "Ratio H/L", log2-transformed and, if necessary, inverted (see

Table EV1). SILAC ratios were corrected for differences in the amount of heavy-labeled and light-labeled cells. In addition, proline containing peptides were corrected for signal loss caused by the conversion of heavy-labeled arginine to heavy-labeled proline (Ong et al, 2003). Normalization factors were calculated independently for each replicate and experiment. For calculation of normalization factors, only unphosphorylated peptides were considered. First, the average log2 ratio of peptides, not containing proline, was calculated and subtracted from the log2 ratios of individual phosphorylated and unphosphorylated peptides. Second, a proline-conversion factor was calculated as the average log2 ratio of unphosphorylated peptides containing exactly one proline and the log2 ratio (divided by two) of peptides containing two prolines. For each phosphorylated and unphosphorylated peptide, the proline-conversion factor was multiplied by the number of prolines present in the peptide sequence and subtracted from the log2 ratio. To correct for differences in protein abundances of Gis1 and Rph1 in the HB purification experiments, all peptides of the respective protein were normalized by subtracting the median log2 ratio of the unphosphorylated peptides. An isoform phosphorylation site probability was calculated by multiplying the highest individual phosphorylation site probabilities. Peptides with an isoform probability below 70% were discarded. To facilitate interpretation of protein phosphorylation sites, phosphopeptides were grouped into "phosphorylation sites" containing the same set of phosphorylated protein residues, regardless of potential missed cleavages or additional modifications such as oxidation. The SILAC log2 ratio of individual "phosphorylation sites" was calculated independently for each replicate and experiment as the average log2 ratio of all corresponding evidence table entries. The replicate ratios were then averaged for the final ratio of the "phosphorylation site".

For analysis of the HB purification experiments, peptides were sorted into "phosphoislands" (Langella et al, 2017; Repetto et al, 2018) that contain adjacent phosphorylation sites covered by overlapping peptides (Dataset EV2). Phosphoislands were generated by grouping phosphopeptides that overlap by at least one of the phosphorylated amino acids. The amino acid sequence and number of phosphosites may vary between the overlapping peptides. For each phosphoisland, one or multiple phosphorylation sites and one unphosphorylated counter group (UCG) were defined, which contains all unphosphorylated peptides that overlap with at least one of the phosphoisland's phosphorylation sites. The SILAC log2 ratios of individual UCGs were calculated as described for phosphorylation sites.

Integration of published mass spectrometry datasets without raw data re-analysis

For integration of the dataset characterizing the effect of Cdc28 inhibition on the phosphorylome, we used in-house Python scripts (see Data and Code Availability section). SILAC ratios were extracted from Kanshin et al (2017) "Supplemental Table S1", using the column "t-test Difference_CDK", and integrated into Dataset EV1 as "Setup Cdc28 inhibition".

Selection of sites for mutational analysis

Phosphorylation sites for mutational analysis were selected according to whether they become increasingly induced by Cdc55 depletion in a time-dependent manner and are also found to be induced in setup SR. Only two phosphorylation sites on each protein fulfilled these strict criteria, Ser[425] and Ser[690] of Gis1 and Ser[412] and Ser[430] of Rph1. Given that both proteins are paralogues, regulated phosphorylation sites that are conserved between these proteins could also be potentially interesting (Strumillo et al, 2019), i.e., Ser[425] of Gis1 being homologous to Ser[430] of Rph1. Ser[405] of Gis1 (homologue to Ser[412] of Rph1) and Ser[584] of Rph1 (homologue to Gis1 Ser[690]) were therefore also included in the mutational analysis. The MS data suggest Cdc55 dependency for both of these phosphorylation sites. Moreover, Ser[405] of Gis1 and Ser[412] of Rph1 lie in a conserved cluster of three juxtaposed phospho-accepting residues with occasional ambiguous phosphorylation site allocation in some peptide hits. An additional serine-to-alanine mutation was therefore introduced in this cluster, namely at Ser[403] of Gis1 and at Ser[410] of Rph1. A second conserved cluster affected by both stress and Cdc55 depletion was observed, however, with decreasing phosphorylation levels (at Ser[696] of Gis1 and Ser[590] of Rph1) in response to the experimental conditions.

Fluorescence-activated cell sorting (FACS) analysis of DNA content

For FACS analysis, 1 ml of early log-phase cells was harvested by centrifugation and fixed with 1 ml 70% ethanol for 3 h at room temperature. Fixed cells were pelleted by centrifugation (1 min, $12,000 \times g$), resuspended in 0.5 ml RNase buffer (50 mM Tris/HCL (pH 7.5), 200 µg/ml RNase A) and incubated overnight at 30°C. Cells were pelleted by centrifugation (1 min, $12,000 \times g$), resuspended in 0.5 ml FACS buffer (50 mM Tris/HCL (pH 7.5), 55 µg/ml propidium iodide) and incubated for 1 h at room temperature. After sonication with 5 short pulses (20% of max output), 20 µl of the cell suspension was diluted in 1 ml 50 mM Tris/HCL (pH 7.5). For each sample, 10,000 cells were analyzed using a FACSCalibur cell analyzer (BD Biosciences). Data were analyzed using FlowCytometryTools (version 0.4.6), a python package for visualization and analysis of high-throughput flow cytometry data (Data ref: Yurtsev & Friedman, 2015). We specifically looked at the FL3-H channel values and normalized the data to the respective 2C peak. For visualization purposes, a Gaussian density curve was laid over the histogram values.

Protein–protein proximity assay (M-Track)

For M-track assays (Zuzuarregui et al, 2012; Brezovich et al, 2015), protein extraction was carried out in RLB+ buffer (1× PBS, 10% glycerol, 0.5% Tween 20, 1 mM NaF, 20 mM ß-glycerophosphate, 1 mM PMSF, 1 mM Na-vanadate, protease inhibitor cocktail (Roche)) at 4°C. Cell extracts were prepared by glass bead lysis using a Fast Prep 24 instrument (MP Biomedicals) with the following settings: 3× 30 s, power level 5.5. Prey proteins were enriched by immunoprecipitation using Dynabeads Pan Mouse IgG (Thermo Fisher Scientific). After washing with RLB+ and RLB buffer (1× PBS, 10% glycerol, 0.5% Tween 20, 1 mM NaF, 20 mM ß-glycerophosphate, 1 mM PMSF, 1 mM Na-vanadate), prey proteins were eluted by boiling for 1 min in 2× urea sample buffer (8 M urea, 80 mM Tris/HCl pH 6.8, 2 mM EDTA pH 8, 2% β-mercaptoethanol, 4% SDS, 4% glycerol). Eluates were analyzed by Western blotting. Histone H3 lysine 9 trimethylation (me3K9H3) of protA-H3-HA tags was visualized using an antibody recognizing me3K9H3 (1:2,000 dilution in 1% yeast

extract (YE) in PBS-T, Novus #NBP1–30141—note: we observed strong differences in the quality and specificity of the antibody between different batches; different batches were used in series 1 and series 2). Membranes were incubated with primary antibody for 1 h at 4 °C, followed by 1 h incubation at 4 °C with HRP-conjugated goat anti-mouse (1:5,000 dilution in 1% YE in PBS-T, Bio-Rad #170–6516) secondary antibody. No washing steps were performed between primary and secondary antibody incubation. Loading was controlled using an antibody recognizing HA (1:5,000 in PBS-T, 12CA5). PicoECL (Thermo Scientific) was used for enhanced chemiluminescent (ECL) detection.

Peak areas of me3K9H3 and HA signals were determined by densitometric analysis of scanned Western blot films using ImageJ and log2-transformed. Each Western blot experiment contained a four-point dilution series of a control sample. A second-degree (series 1) or first-degree (series 2) polynomial curve was fitted independently to the me3K9H3 and HA signals of to the dilution series, which was used to correct me3K9H3 and HA signals for unequal loading amounts between samples and to normalize between different Western blot experiments. Proximity signals were calculated as the difference of the normalized log2-transformed me3K9H3 and HA signal intensity and rescaled by subtracting the mean proximity signal of the negative control (Cdc55-protA-H3-HA, no HKMT). A one-tailed Welch's t-test was used to identify the statistically significant candidates. For each candidate, the proximity signal of all replicates was compared against all proximity signals of the negative control (Cdc55-protA-H3-HA, no HKMT). P-values were corrected for multiple testing by using the Benjamini–Hochberg procedure to generate q-values.

M-track protein–protein proximity analysis of yeast strains GG628 (*rim15Δ*, *GIS1*-HKMT, *CDC55*-protA-H3HA) and GG630 (*rim15Δ*, *RPH1*-HKMT, *CDC55*-protA-H3HA, Fig 5B) was carried out using MES lysis buffer (50 mM MES/NaOH pH 6.5, 150 mM NaOH, 1% Triton, 1 mM EDTA, complete EDTA free (Roche)). Cell extracts were prepared by glass bead lysis using a Fast Prep 24 instrument (MP Biomedicals) with the following settings: 1 × 45 s, power level 6.5. Immunoprecipitation of prey proteins was achieved using anti-HA-magnetic beads (Pierce). Washing steps were carried out using a MES-wash buffer (50 mM MES/NaOH pH 6.5, 150 mM NaOH, 1 mM EDTA). Prey proteins were eluted by heat incubation in a 2× urea sample buffer. Each sample was mixed with 4 μl of a HeLa lysate (protein concentration 1 mg/ml in urea sample buffer) before loading in order to improve Western blot transfer efficiency rates.

Phospho-shift assay

Cell lysis was carried out in MES lysis buffer (50 mM MES/NaOH pH 6.5, 150 mM NaOH, 1% Triton, 1 mM EDTA, Complete EDTA free (Roche)) by beating using a Fast Prep 24 instrument (MP Biomedicals) with the following settings: 3 × 45 s, power level 6.5. Cleared protein extracts were resolved in SDS–PAGE loading buffer (62.5 mM Tris–HCl (pH 6.8), 8 M urea, 2% (w/v) SDS, 0.05% (w/v) bromophenol blue, 10% (v/v) glycerol, 5% (v/v) β-mercaptoethanol) and incubated at 95°C for 1 min. For Mn^{2+}-Phos-tag SDS–PAGE, 25 μM of Phos-tag-AAL (Wako) and 50 μM of $MnCl_2$ were added to the separating gel before polymerization. The pH of the separation gel was adjusted to 8 for Mn^{2+}-Phos-tag SDS–PAGE and 8.8 for standard SDS–PAGE. Gelshifts were visualized by

Western blot using an antibody recognizing HA (12CA5). Hyperosmotic stress was controlled by monitoring phosphorylation of MAPK Hog1 using an antibody against phospho-p38 (Cell Signaling, Phospho-p38 MAPK (Thr180/Tyr182) Antibody #9211, 1:5,000), protein levels of Cdc55 by using an antibody against Cdc55 (Max Perutz Labs Vienna, Monoclonal Antibody Facility, 1:200 (Zuzuarregui *et al*, 2012)). Loading was controlled using an antibody recognizing Cdc28 (HPA030762, Sigma-Aldrich, 1:10,000).

Gene expression analysis

Total RNA isolation was adapted from Cross and Tinkelenberg (Cross & Tinkelenberg, 1991). 20 ml of early log-phase cells was harvested by centrifugation (2 min, $4 \times g$, 4°C) and resuspended in 200 μl TE buffer. Cell breakage was performed using approximately 200 μl glass beads and 200 μl phenol–chloroform–isopropanol (25:24:1 in 10 mM Tris/HCl, pH 8.0) in a Fast Prep 24 instrument (MP Biomedicals) for 2 × 10 s at power level 6. After centrifugation (15 min, $20,000 \times g$, 4°C), the upper aqueous phase was washed twice (mixed and centrifuged 10 min, $20,000 \times g$, 4°C) with an equal volume of chloroform–isopropanol (24:1). 100 μl of the aqueous phase was transferred to a new tube; precipitation was performed in 0.04 M sodium acetate, 64% ethanol. Samples were incubated for 30 min or overnight at −20°C. RNA was pelleted (10 min, $20,000 \times g$, 4°C), supernatant was removed completely, and the RNA pellet was resuspended in 50 μl ddH_2O to yield an RNA concentration of 4–8 μg/μl. RNA samples were treated with RNase-free DNase (Thermo Fisher, 1 U/μg RNA) at 37°C for 30 min, the reaction was stopped by adding 1 μl of 50 mM EDTA at 65°C for 10 min, and cDNA was synthesized using GoScript Reverse Transcriptase (Promega) with oligo(dT) primers (Microsynth). RT-qPCR analyses were performed on cDNA templates using RT-qPCR master mix containing SYBR Green I nucleic acid gel stain (Sigma) for the time-course experiments and LUNA master mix (NEB) for the 30 min time point experiments on 96-well plates in a Mastercycler Realplex 2 (Eppendorf). The following gene-specific primers were used. *CTT1* Fw: AAT CAG TTT CAG GAC ACT ACC, *CTT1* Rv: GAA TGA CCA GAG TAC GCG TTC, *PGM2* Fw: CTC TGG TTT GCG TAA GAA GAC, *PGM2* Rv: TTG TAG TAA CGC CCA TCA CC, *IPP1* Fw: GAT GGT AAG CCA GTT TCT GC, *IPP1* Rv: GGT TCA AAG TTT CTT CCT TGG. Specificity of RT-qPCRs was verified by agarose gel electrophoresis and melting curve analysis. A single band of the expected size and a single peak, respectively, were required. Quality of mRNA was analyzed on Agilent 2100 Bioanalyzer Instrument (Assay Class: Eukaryote Total RNA Nano, version 2.6) and confirmed to constitute RIN values of > 7 for all 30 min time point samples (Appendix Fig S3A and B). Additionally, amplification efficiencies for each target gene (*CTT1*, *PGM2*) and the reference gene (*IPP1*) in LUNA master mix (NEB) were determined by standard curves obtained from serial dilution reactions and reached > 90%. Gene expression data were collected from at least 3 biological replicates and technical duplicates (time-course data) or triplicates (30 min time point data) per sample. LG *Cq* values (averaged over technical replicates) of target genes were corrected for efficiency of the respective assay, and gene expression levels were determined by relative quantification based on the *Cq* values of the reference gene in the same sample (Δ*Cq* method). All datasets (one set = all samples per biological replicate) were evaluated

individually for technical integrity by checking for extreme outliers, failed individual reactions, and missing data, and were considered valid if more than 75% of the reaction plate were uncompromised. Each valid biological replicate was then normalized over the sum of all values that were uncompromised across the entire experiment and integrated to compare expression levels between samples.

Determination of growth rates

Growth curves were fitted using the GROFIT package in R (Kahm *et al*, 2010). GROFIT was used to calculate the growth rate μ $[h^{-1}]$ from each growth curve. Growth rates were then given as mean ± standard deviation of triplicates. Underlying data are shown in Dataset EV4.

Serial dilution droplet test

W303-1A wild-type and deletion mutant strains were grown to mid-log phase. $OD_{600 \text{ nm}}$ values of cultures were equalized to 0.1, and serial dilution steps of 1:7 dilutions were prepared. Droplets of 2.5 μl were transferred onto a hyperosmotic stress (YPD +0.8 M NaCl) and onto a YPD plate with no additives as a control. Plates were incubated at 30°C, and growth was monitored for 4 days.

GO-term analysis

GO enrichment analysis was performed with DAVID (version 6.8) (https://david.ncifcrf.gov/) (Huang *et al*, 2009), based on GO terms "Biological Process" with GO hierarchy levels ranging from level 3–6. Only gene ontology terms with corrected $P < 0.05$ are considered.

MotifX and threonine enrichment

We used the MotifX algorithm implemented in R (Schwartz & Gygi, 2005; Chou & Schwartz, 2011; Wagih *et al*, 2016) to identify over-represented linear motifs within specific sets of phosphorylation sites. A sequence window of 13 residues (± 6 residues around the phosphorylated amino acid) was selected to extract phosphorylation motifs. Serine and threonine containing phosphorylation sites were analyzed independently of each other. In case of multiple phosphorylated sites per peptide, each phosphorylated residue was considered individually. The following settings were used to run the R script: minimal sequences 20, *P*-value cutoff 0.01. For the threonine enrichment analysis, the MotifX input sequences were used and Fisher's exact test was applied to assess statistical significance.

Data availability

The datasets produced in this study and the scripts used for data analysis are available in the following databases:

- Phospho-proteomic MS data: PRIDE PXD019646 (http://www.eb i.ac.uk/pride/archive/projects/PXD019646).
- Python scripts used for data analysis: GitHub (https://github. com/hollenstein/sourcecode_cdc55).

Expanded View for this article is available online.

Author contributions

DMH and WR conceptualized the study. DMH, CS, EO, GA, and WR designed experiments. DMH, GG, NR, JF, JV, RB, CS, and WR performed experiments. DMH, NR, MJ, CS, and MH analyzed the data. DMH, NR, and WR wrote the paper. All authors edited the text. All authors read and approved the final manuscript.

Conflict of interest

The authors declare that they have no conflict of interest.

References

Agostinis P, Goris J, Pinna LA, Marchiori F, Perich JW, Meyer HE, Merlevede W (1990) Synthetic peptides as model substrates for the study of the specificity of the polycation-stimulated protein phosphatases. *Eur J Biochem* 189: 235–241

Álvarez-Fernández M, Sanz-Flores M, Sanz-Castillo B, Salazar-Roa M, Partida D, Zapatero-Solana E, Ali HR, Manchado E, Lowe S, VanArsdale T *et al* (2018) Therapeutic relevance of the PP2A-B55 inhibitory kinase MASTL/ Greatwall in breast cancer. *Cell Death Differ* 25: 828–840

Apostolidis SA, Rodríguez-Rodríguez N, Suárez-Fueyo A, Dioufa N, Ozcan E, Crispín JC, Tsokos MG, Tsokos GC (2016) Phosphatase PP2A is requisite for the function of regulatory T cells. *Nat Immunol* 17: 556–564

Bao YI, Oguz G, Lee WC, Lee PL, Ghosh K, Li J, Wang P, Lobie PE, Ehmsen S, Ditzel HJ *et al* (2020) EZH2-mediated PP2A inactivation confers resistance to HER2-targeted breast cancer therapy. *Nat Commun* 11: 5878

Belazzi T, Wagner A, Wieser R, Schanz M, Adam G, Hartig A, Ruis H (1991) Negative regulation of transcription of the *Saccharomyces cerevisiae* catalase T (CTT1) gene by cAMP is mediated by a positive control element. *EMBO J* 10: 585–592

Blume-Jensen P, Hunter T (2001) Oncogenic kinase signalling. *Nature* 411: 355–365

Bontron S, Jaquenoud M, Vaga S, Talarek N, Bodenmiller B, Aebersold R, De Virgilio C (2013) Yeast endosulfines control entry into quiescence and chronological life span by inhibiting protein phosphatase 2A. *Cell Rep* 3: 16–22

Brautigan DL (2013) Protein Ser/Thr phosphatases–the ugly ducklings of cell signalling. *FEBS J* 280: 324–345

Brewster JL, Gustin MC (2014) Hog 1: 20 years of discovery and impact. *Sci Signal* 7: re7

Brezovich A, Schuschnig M, Ammerer G, Kraft C (2015) An *in vivo* detection system for transient and low-abundant protein interactions and their kinetics in budding yeast. *Yeast* 32: 355–365

Castro A, Lorca T (2018) Greatwall kinase at a glance. *J Cell Sci* 131: jcs222364

Chan LY, Amon A (2009) The protein phosphatase 2A functions in the spindle position checkpoint by regulating the checkpoint kinase Kin4. *Genes Dev* 23: 1639–1649

Chou MF, Schwartz D (2011) Biological sequence motif discovery using motif-x. *Current protocols in bioinformatics*. Hoboken, NJ: John Wiley & Sons, Inc., p. Unit 13.15-24

Courtney TM, Deiters A (2019) Optical control of protein phosphatase function. *Nat Commun* 10: 4384

Cox J, Mann M (2008) MaxQuant enables high peptide identification rates, individualized p.p.b.-range mass accuracies and proteome-wide protein quantification. *Nat Biotechnol* 26: 1367–1372

Creamer TP (2020) Calcineurin. Cell Commun. *Signal* 18: 137

Cross FR, Tinkelenberg AH (1991) A potential positive feedback loop controlling CLN1 and CLN2 gene expression at the start of the yeast cell cycle. *Cell* 65: 875–883

Cundell MJ, Hutter LH, Nunes Bastos R, Poser E, Holder J, Mohammed S, Novak B, Barr FA (2016) A PP2A-B55 recognition signal controls substrate dephosphorylation kinetics during mitotic exit. *J Cell Biol* 214: 539–554

Eidenmüller J, Fath T, Maas T, Pool M, Sontag E, Brandt R (2001) Phosphorylation-mimicking glutamate clusters in the proline-rich region are sufficient to simulate the functional deficiencies of hyperphosphorylated tau protein. *Biochem J* 357: 759–767

Evangelista CC, Rodriguez Torres AM, Limbach MP, Zitomer RS (1996) Rox3 and Rts1 function in the global stress response pathway in baker's yeast. *Genetics* 142: 1083–1093

Fabbrizi MR, Meyer B, Misri S, Raj S, Zobel CL, Hallahan DE, Sharma GG (2018) Transient PP2A inhibition alleviates normal tissue stem cell susceptibility to cell death during radiotherapy. *Cell Death Dis* 9: 492

Fahs S, Lujan P, Köhn M (2016) Approaches to study phosphatases. *ACS Chem Biol* 11: 2944–2961

Ferrari E, Bruhn C, Peretti M, Cassani C, Carotenuto WV, Elgendy M, Shubassi G, Lucca C, Bermejo R, Varasi M *et al* (2017) PP2A controls genome integrity by integrating nutrient-sensing and metabolic pathways with the DNA damage response. *Mol Cell* 67: 266–281.e4

Ficarro SB, McCleland ML, Stukenberg PT, Burke DJ, Ross MM, Shabanowitz J, Hunt DF, White FM (2002) Phosphoproteome analysis by mass spectrometry and its application to *Saccharomyces cerevisiae*. *Nat Biotechnol* 20: 301–305

François J, Parrou JL (2001) Reserve carbohydrates metabolism in the yeast *Saccharomyces cerevisiae*. *FEMS Microbiol Rev* 25: 125–145

García-Blanco N, Vázquez-Bolado A, Moreno S (2019) Greatwall-Endosulfine: a molecular switch that regulates PP2A/B55 protein phosphatase activity in dividing and quiescent cells. *Int J Mol Sci* 20: 6228

García-Rodríguez LJ, Valle R, Durán A, Roncero C (2005) Cell integrity signaling activation in response to hyperosmotic shock in yeast. *FEBS Lett* 579: 6186–6190

Gasch AP, Spellman PT, Kao CM, Carmel-Harel O, Eisen MB, Storz G, Botstein D, Brown PO (2000) Genomic expression programs in the response of yeast cells to environmental changes. *Mol Biol Cell* 11: 4241–4257

Gharbi-Ayachi A, Labbé J-C, Burgess A, Vigneron S, Strub J-M, Brioudes E, Van-Dorsselaer A, Castro A, Lorca T (2010) The substrate of Greatwall kinase, Arpp19, controls mitosis by inhibiting protein phosphatase 2A. *Science* 330: 1673–1677

Godfrey M, Touati SA, Kataria M, Jones A, Snijders AP, Uhlmann F (2017) PP2ACdc55 phosphatase imposes ordered cell-cycle phosphorylation by opposing threonine phosphorylation. *Mol Cell* 65: 393–402.e3

Gruhler A, Olsen JV, Mohammed S, Mortensen P, Faergeman NJ, Mann M, Jensen ON (2005) Quantitative phosphoproteomics applied to the yeast pheromone signaling pathway. *Mol Cell Proteomics* 4: 310–327

Grundke-Iqbal I, Iqbal K, Tung YC, Quinlan M, Wisniewski HM, Binder LI (1986) Abnormal phosphorylation of the microtubule-associated protein tau (tau) in Alzheimer cytoskeletal pathology. *Proc Natl Acad Sci USA* 83: 4913–4917

Hao N, Zeng Y, Elston TC, Dohlman HG (2008) Control of MAPK specificity by feedback phosphorylation of shared adaptor protein Ste50. *J Biol Chem* 283: 33798–33802

Hentges P, Van Driessche B, Tafforeau L, Vandenhaute J, Carr AM (2005) Three novel antibiotic marker cassettes for gene disruption and marker switching in *Schizosaccharomyces pombe*. *Yeast* 22: 1013–1019

Hohmann S (2002) Osmotic stress signaling and osmoadaptation in yeasts. *Microbiol Mol Biol Rev* 66: 300–372

Hollenstein DM, Veis J, Romanov N, Gerecova G, Ogris E, Hartl M, Ammerer G, Reiter W (2020) PP2A-Rts1 antagonizes Rck2-mediated hyperosmotic stress signaling in yeast. *BioRxiv* https://doi.org/10.1101/2020.05.30.124925 [PREPRINT]

Huang DW, Sherman BT, Lempicki RA (2009) Systematic and integrative analysis of large gene lists using DAVID bioinformatics resources. *Nat Protoc* 4: 44–57

Huh W-K, Falvo JV, Gerke LC, Carroll AS, Howson RW, Weissman JS, O'Shea EK (2003) Global analysis of protein localization in budding yeast. *Nature* 425: 686–691

Janschitz M, Romanov N, Varnavides G, Hollenstein DM, Gérecová G, Ammerer G, Hartl M, Reiter W (2019) Novel interconnections of HOG signaling revealed by combined use of two proteomic software packages. *Cell Commun Signal* 17: 66

Játiva S, Calabria I, Moyano-Rodriguez Y, Garcia P, Queralt E (2019) Cdc14 activation requires coordinated Cdk1-dependent phosphorylation of Net1 and PP2A-Cdc55 at anaphase onset. *Cell Mol Life Sci* 76: 3601–3620

Jin N, Jin Y, Weisman LS (2017) Early protection to stress mediated by CDK-dependent PI3,5P2 signaling from the vacuole/lysosome. *J Cell Biol* 216: 2075–2090

Juanes MA, Khoueiry R, Kupka T, Castro A, Mudrak I, Ogris E, Lorca T, Piatti S (2013) Budding yeast greatwall and endosulfines control activity and spatial regulation of PP2A(Cdc55) for timely mitotic progression. *PLoS Genet* 9: e1003575

Kahm M, Hasenbrink G, Lichtenberg-Fraté H, Ludwig J, Kschischo M (2010) grofit: Fitting Biological Growth Curves with R. *J. Stat. Softw.* 33.

Kanshin E, Bergeron-Sandoval L-P, Isik SS, Thibault P, Michnick SW (2015) A cell-signaling network temporally resolves specific versus promiscuous phosphorylation. *Cell Rep* 10: 1202–1214

Kanshin E, Giguère S, Jing C, Tyers M, Thibault P (2017) Machine learning of global phosphoproteomic profiles enables discrimination of direct versus indirect kinase substrates. *Mol Cell Proteomics* 16: 786–798

Kauko O, O'Connor CM, Kulesskiy E, Sangodkar J, Aakula A, Izadmehr S, Yetukuri L, Yadav B, Padzik A, Laajala TD *et al* (2018) PP2A inhibition is a druggable MEK inhibitor resistance mechanism in KRAS-mutant lung cancer cells. *Sci Transl Med* 10: eaaq1093

Kelliher CM, Foster MW, Motta FC, Deckard A, Soderblom EJ, Moseley MA, Haase SB (2018) Layers of regulation of cell-cycle gene expression in the budding yeast *Saccharomyces cerevisiae*. *Mol Biol Cell* 29: 2644–2655

Keshava Prasad TS, Goel R, Kandasamy K, Keerthikumar S, Kumar S, Mathivanan S, Telikicherla D, Raju R, Shafreen B, Venugopal A *et al* (2009) Human protein reference database–2009 update. *Nucleic Acids Res* 37: D767–D772

Khanna A, Pimanda JE, Westermarck J (2013) Cancerous inhibitor of protein phosphatase 2A, an emerging human oncoprotein and a potential cancer therapy target. *Cancer Res* 73: 6548−6553

Kinoshita E, Kinoshita-Kikuta E, Takiyama K, Koike T (2006) Phosphate-binding tag, a new tool to visualize phosphorylated proteins. *Mol Cell Proteomics* 5: 749−757

Klopf E, Paskova L, Solé C, Mas G, Petryshyn A, Posas F, Wintersberger U, Ammerer G, Schüller C (2009) Cooperation between the INO80 complex and histone chaperones determines adaptation of stress gene transcription in the yeast *Saccharomyces cerevisiae*. *Mol Cell Biol* 29: 4994−5007

Knop M, Siegers K, Pereira G, Zachariae W, Winsor B, Nasmyth K, Schiebel E (1999) Epitope tagging of yeast genes using a PCR-based strategy: more tags and improved practical routines. *Yeast* 15: 963−972

Köhn M (2020) Turn and face the strange: a new view on phosphatases. *ACS Cent Sci* 6: 467−477

Kruse T, Gnosa SP, Nasa I, Garvanska DH, Hein JB, Nguyen H, Samsøe-Petersen J, Lopez-Mendez B, Hertz EPT, Schwarz J *et al* (2020) Mechanisms of site-specific dephosphorylation and kinase opposition imposed by PP2A regulatory subunits. *EMBO J* 39: e103695

Langella O, Valot B, Balliau T, Blein-Nicolas M, Bonhomme L, Zivy M (2017) X! TandemPipeline: a tool to manage sequence redundancy for protein inference and phosphosite identification. *J Proteome Res* 16: 494−503

Leslie SN, Nairn AC (2019) cAMP regulation of protein phosphatases PP1 and PP2A in brain. *Biochim Biophys Acta Mol Cell Res* 1866: 64−73

Liang C-Y, Wang L-C, Lo W-S (2013) Dissociation of the H3K36 demethylase Rph1 from chromatin mediates derepression of environmental stress-response genes under genotoxic stress in *Saccharomyces cerevisiae*. *Mol Biol Cell* 24: 3251−3262

Marchler G, Schüller C, Adam G, Ruis H (1993) A *Saccharomyces cerevisiae* UAS element controlled by protein kinase A activates transcription in response to a variety of stress conditions. *EMBO J* 12: 1997−2003

Mazhar S, Taylor SE, Sangodkar J, Narla G (2019) Targeting PP2A in cancer: combination therapies. *Biochim Biophys Acta Mol Cell Res* 1866: 51−63

McClinch K, Avelar RA, Callejas D, Izadmehr S, Wiredja D, Perl A, Sangodkar J, Kastrinsky DB, Schlatzer D, Cooper M *et al* (2018) Small-molecule activators of protein phosphatase 2A for the treatment of castration-resistant prostate cancer. *Cancer Res* 78: 2065−2080

Meeusen B, Janssens V (2018) Tumor suppressive protein phosphatases in human cancer: emerging targets for therapeutic intervention and tumor stratification. *Int J Biochem Cell Biol* 96: 98−134

Mendenhall MD, Hodge AE (1998) Regulation of Cdc28 cyclin-dependent protein kinase activity during the cell cycle of the yeast *Saccharomyces cerevisiae*. *Microbiol Mol Biol Rev* 62: 1191−1243

Meyerovitch J, Backer JM, Kahn CR (1989) Hepatic phosphotyrosine phosphatase activity and its alterations in diabetic rats. *J Clin Invest* 84: 976−983

Minshull J, Straight A, Rudner AD, Dernburg AF, Belmont A, Murray AW (1996) Protein phosphatase 2A regulates MPF activity and sister chromatid cohesion in budding yeast. *Curr Biol* 6: 1609−1620

Mishra A, Oulès B, Pisco AO, Ly T, Liakath-Ali K, Walko G, Viswanathan P, Tihy M, Nijjher J, Dunn S-J *et al* (2017) A protein phosphatase network controls the temporal and spatial dynamics of differentiation commitment in human epidermis. *Elife* 6: 1−20

Mochida S, Hunt T (2012) Protein phosphatases and their regulation in the control of mitosis. *EMBO Rep* 13: 197−203

Mochida S, Ikeo S, Gannon J, Hunt T (2009) Regulated activity of PP2A-B55 delta is crucial for controlling entry into and exit from mitosis in Xenopus egg extracts. *EMBO J* 28: 2777−2785

Mochida S, Maslen SL, Skehel M, Hunt T (2010) Greatwall phosphorylates an inhibitor of protein phosphatase 2A that is essential for mitosis. *Science* 330: 1670−1673

Moore SD, Prevelige PE (2002) A P22 scaffold protein mutation increases the robustness of head assembly in the presence of excess portal protein. *J Virol* 76: 10245−10255

Morawska M, Ulrich HD (2013) An expanded tool kit for the auxin-inducible degron system in budding yeast. *Yeast* 30: 341−351

Moreno-Torres M, Jaquenoud M, De Virgilio C (2015) TORC1 controls G1-S cell cycle transition in yeast via Mpk1 and the greatwall kinase pathway. *Nat Commun* 6: 8256

Moyano-Rodriguez Y, Queralt E (2019) PP2A functions during mitosis and cytokinesis in yeasts. *Int J Mol Sci* 21: 264

Needham EJ, Parker BL, Burykin T, James DE, Humphrey SJ (2019) Illuminating the dark phosphoproteome. *Sci Signal* 12: eaau8645

Nishimura K, Fukagawa T, Takisawa H, Kakimoto T, Kanemaki M (2009) An auxin-based degron system for the rapid depletion of proteins in nonplant cells. *Nat Methods* 6: 917−922

Nishizawa M, Tanigawa M, Hayashi M, Maeda T, Yazaki Y, Saeki Y, Toh-e A (2010) Pho85 kinase, a cyclin-dependent kinase, regulates nuclear accumulation of the Rim101 transcription factor in the stress response of *Saccharomyces cerevisiae*. *Eukaryot Cell* 9: 943−951

O'Connor CM, Perl A, Leonard D, Sangodkar J, Narla G (2018) Therapeutic targeting of PP2A. *Int J Biochem Cell Biol* 96: 182−193

Ong S-E, Blagoev B, Kratchmarova I, Kristensen DB, Steen H, Pandey A, Mann M (2002) Stable isotope labeling by amino acids in cell culture, SILAC, as a simple and accurate approach to expression proteomics. *Mol Cell Proteomics* 1: 376−386

Ong S-E, Kratchmarova I, Mann M (2003) Properties of 13 C-substituted arginine in stable isotope labeling by amino acids in cell culture (SILAC). *J Proteome Res* 2: 173−181

Ozcan U, Cao Q, Yilmaz E, Lee A-H, Iwakoshi NN, Ozdelen E, Tuncman G, Görgün C, Glimcher LH, Hotamisligil GS (2004) Endoplasmic reticulum stress links obesity, insulin action, and type 2 diabetes. *Science* 306: 457−461

Park H-S, Lee SC, Cardenas ME, Heitman J (2019) Calcium-calmodulin-calcineurin signaling: a globally conserved virulence cascade in eukaryotic microbial pathogens. *Cell Host Microbe* 26: 453−462

Park MC, Kang T, Jin D, Han JM, Kim SB, Park YJ, Cho K, Park YW, Guo M, He W *et al* (2012) Secreted human glycyl-tRNA synthetase implicated in defense against ERK-activated tumorigenesis. *Proc Natl Acad Sci USA* 109: E640−E647

Perrotti D, Neviani P (2008) Protein phosphatase 2A (PP2A), a drugable tumor suppressor in Ph1(+) leukemias. *Cancer Metastasis Rev* 27: 159−168

Pierce M, Wagner M, Xie J, Gailus-Durner V, Six J, Vershon AK, Winter E (1998) Transcriptional regulation of the SMK1 mitogen-activated protein kinase gene during meiotic development in *Saccharomyces cerevisiae*. *Mol Cell Biol* 18: 5970−5980

Queralt E, Lehane C, Novak B, Uhlmann F (2006) Downregulation of PP2A (Cdc55) phosphatase by separase initiates mitotic exit in budding yeast. *Cell* 125: 719−732

Rappsilber J, Mann M, Ishihama Y (2007) Protocol for micro-purification, enrichment, pre-fractionation and storage of peptides for proteomics using StageTips. *Nat Protoc* 2: 1896−1906

Reiter W, Anrather D, Dohnal I, Pichler P, Veis J, Grøtli M, Posas F, Ammerer G (2012) Validation of regulated protein phosphorylation events in yeast by quantitative mass spectrometry analysis of purified proteins. *Proteomics* 12: 3030−3043

Reiter W, Klopf E, De Wever V, Anrather D, Petryshyn A, Roetzer A, Niederacher G, Roitinger E, Dohnal I, Görner W et al (2013) Yeast protein phosphatase 2A-Cdc55 regulates the transcriptional response to hyperosmolarity stress by regulating Msn2 and Msn4 chromatin recruitment. Mol Cell Biol 33: 1057–1072

Rep M, Reiser V, Gartner U, Thevelein JM, Hohmann S, Ammerer G, Ruis H (1999) Osmotic stress-induced gene expression in Saccharomyces cerevisiae requires Msn1p and the novel nuclear factor Hot1p. Mol Cell Biol 19: 5474–5485

Repetto MV, Winters MJ, Bush A, Reiter W, Hollenstein DM, Ammerer G, Pryciak PM, Colman-Lerner A (2018) CDK and MAPK synergistically regulate signaling dynamics via a shared multi-site phosphorylation region on the scaffold protein Ste5. Mol Cell 69: 938–952.e6

Rikova K, Guo A, Zeng Q, Possemato A, Yu J, Haack H, Nardone J, Lee K, Reeves C, Li YU et al (2007) Global survey of phosphotyrosine signaling identifies oncogenic kinases in lung cancer. Cell 131: 1190–1203

Romanov N, Hollenstein DM, Janschitz M, Ammerer G, Anrather D, Reiter W (2017) Identifying protein kinase-specific effectors of the osmostress response in yeast. Sci Signal 10: eaag2435

Romanov N, Hollenstein DM, Janschitz M, Ammerer G, Anrather D, Reiter W (2017) Identifying protein kinase specific effectors of the osmostress response in yeast_part1 - part7. PRoteomics Identif. Database PRIDE https://www.ebi.ac.uk/pride/archive/projects/PXD004294 PXD004294-PXD004300 [DATASET]

Sadowski I, Breitkreutz B-J, Stark C, Su T-C, Dahabieh M, Raithatha S, Bernhard W, Oughtred R, Dolinski K, Barreto K et al (2013) The PhosphoGRID Saccharomyces cerevisiae protein phosphorylation site database: version 2.0 update. Database 2013: bat026

Saito H, Posas F (2012) Response to hyperosmotic stress. Genetics 192: 289–318

Santhanam A, Hartley A, Düvel K, Broach JR, Garrett S (2004) PP2A phosphatase activity is required for stress and Tor kinase regulation of yeast stress response factor Msn2p. Eukaryot Cell 3: 1261–1271

Sarkar S, Dalgaard JZ, Millar JBA, Arumugam P (2014) The Rim15-endosulfine-PP2ACdc55 signalling module regulates entry into gametogenesis and quiescence via distinct mechanisms in budding yeast. PLoS Genet 10: e1004456

Schwartz D, Gygi SP (2005) An iterative statistical approach to the identification of protein phosphorylation motifs from large-scale data sets. Nat Biotechnol 23: 1391–1398

Shi Y (2009) Serine/threonine phosphatases: mechanism through structure. Cell 139: 468–484

Shu Y, Yang H, Hallberg E, Hallberg R (1997) Molecular genetic analysis of Rts1p, a B′ regulatory subunit of Saccharomyces cerevisiae protein phosphatase 2A. Mol Cell Biol 17: 3242–3253

Smoly I, Shemesh N, Ziv-Ukelson M, Ben-Zvi A, Yeger-Lotem E (2017) An asymmetrically balanced organization of kinases versus phosphatases across eukaryotes determines their distinct impacts. PLoS Comput Biol 13: e1005221

Sontag J-M, Sontag E (2014) Protein phosphatase 2A dysfunction in Alzheimer's disease. Front Mol Neurosci 7: 16

Strumillo MJ, Oplová M, Viéitez C, Ochoa D, Shahraz M, Busby BP, Sopko R, Studer RA, Perrimon N, Panse VG et al (2019) Conserved phosphorylation hotspots in eukaryotic protein domain families. Nat Commun 10: 1977

Tanaka S, Miyazawa-Onami M, Iida T, Araki H (2015) iAID: an improved auxin-inducible degron system for the construction of a "tight" conditional mutant in the budding yeast Saccharomyces cerevisiae. Yeast 32: 567–581

Teixeira MC, Monteiro P, Jain P, Tenreiro S, Fernandes AR, Mira NP, Alenquer M, Freitas AT, Oliveira AL, Sá-Correia I (2006) The YEASTRACT database: a tool for the analysis of transcription regulatory associations in Saccharomyces cerevisiae. Nucleic Acids Res 34: D446–D451

Teixeira MC, Monteiro PT, Palma M, Costa C, Godinho CP, Pais P, Cavalheiro M, Antunes M, Lemos A, Pedreira T et al (2018) YEASTRACT: an upgraded database for the analysis of transcription regulatory networks in Saccharomyces cerevisiae. Nucleic Acids Res 46: D348–D353

Thai V, Dephoure N, Weiss A, Ferguson J, Leitao R, Gygi SP, Kellogg DR (2017) Protein kinase C controls binding of Igo/ENSA proteins to protein phosphatase 2A in budding yeast. J Biol Chem 292: 4925–4941

Thomas BJ, Rothstein R (1989) Elevated recombination rates in transcriptionally active DNA. Cell 56: 619–630

Touati SA, Hofbauer L, Jones AW, Snijders AP, Kelly G, Uhlmann F (2019) Cdc14 and PP2A phosphatases cooperate to shape phosphoproteome dynamics during mitotic exit. Cell Rep 29: 2105–2119.e4

UniProt Consortium (2019) UniProt: a worldwide hub of protein knowledge. Nucleic Acids Res 47: D506–D515

Virshup DM, Shenolikar S (2009) From promiscuity to precision: protein phosphatases get a makeover. Mol Cell 33: 537–545

Vizcaíno J, Csordas A, del-Toro N, Dianes JA, Griss J, Lavidas I, Mayer G, Perez-Riverol Y, Reisinger F, Ternent T et al (2016) 2016 update of the PRIDE database and its related tools. Nucleic Acids Res 44: D447–D456

Vlastaridis P, Kyriakidou P, Chaliotis A, Van de Peer Y, Oliver SG, Amoutzias GD (2017) Estimating the total number of phosphoproteins and phosphorylation sites in eukaryotic proteomes. Gigascience 6: 1–11

Wach A, Brachat A, Pöhlmann R, Philippsen P (1994) New heterologous modules for classical or PCR-based gene disruptions in Saccharomyces cerevisiae. Yeast 10: 1793–1808

Wagih O, Sugiyama N, Ishihama Y, Beltrao P (2016) Uncovering phosphorylation-based specificities through functional interaction networks. Mol Cell Proteomics 15: 236–245

Wandzioch E, Pusey M, Werda A, Bail S, Bhaskar A, Nestor M, Yang J, Rice LM (2014) PME-1 modulates protein phosphatase 2A activity to promote the malignant phenotype of endometrial cancer cells. Cancer Res 74: 4295–4305

Wang Y, Burke DJ (1997) Cdc55p, a B-type regulatory subunit of protein phosphatase 2A, has multiple functions in mitosis and is required for the kinetochore/spindle checkpoint in Saccharomyces cerevisiae. Mol Cell Biol 17: 620–626

Wang Y, Ng T-Y (2006) Phosphatase 2A negatively regulates mitotic exit in Saccharomyces cerevisiae. Mol Biol Cell 17: 80–89

Wanke V, Pedruzzi I, Cameroni E, Dubouloz F, De Virgilio C (2005) Regulation of G0 entry by the Pho80-Pho85 cyclin-CDK complex. EMBO J 24: 4271–4278

Wei H, Ashby DG, Moreno CS, Ogris E, Yeong FM, Corbett AH, Pallas DC (2001) Carboxymethylation of the PP2A catalytic subunit in Saccharomyces cerevisiae is required for efficient interaction with the B-type subunits Cdc55p and Rts1p. J Biol Chem 276: 1570–1577

Westermarck J (2018) Targeted therapies don't work for a reason; the neglected tumor suppressor phosphatase PP2A strikes back. FEBS J 285: 4139–4145

Williams BC, Filter JJ, Blake-Hodek KA, Wadzinski BE, Fuda NJ, Shalloway D, Goldberg ML (2014) Greatwall-phosphorylated Endosulfine is both an inhibitor and a substrate of PP2A-B55 heterotrimers. Elife 3: e01695

Wlodarchak N, Xing Y (2016) PP2A as a master regulator of the cell cycle. Crit Rev Biochem Mol Biol 51: 162–184

Wu J, Tolstykh T, Lee J, Boyd K, Stock JB, Broach JR (2000) Carboxyl methylation of the phosphoprotein phosphatase 2A catalytic subunit promotes its functional association with regulatory subunits *in vivo*. *EMBO J* 19: 5672−5681

Yabe R, Tsuji S, Mochida S, Ikehara T, Usui T, Ohama T, Sato K (2018) A stable association with PME-1 may be dispensable for PP2A demethylation - implications for the detection of PP2A methylation and immunoprecipitation. *FEBS Open Biol* 8: 1486−1496

Yu K, Zhang Q, Liu Z, Zhao QI, Zhang X, Wang Y, Wang Z-X, Jin Y, Li X, Liu Z-X *et al* (2019) qPhos: a database of protein phosphorylation dynamics in humans. *Nucleic Acids Res* 47: D451−D458

Yurtsev E & Friedman J (2015) (https://doi.org/10.5281/zenodo.32992) [DATASET]

Zanivan S, Meves A, Behrendt K, Schoof EM, Neilson LJ, Cox J, Tang HR, Kalna G, van Ree JH, van Deursen JM *et al* (2013) *In vivo* SILAC-based proteomics reveals phosphoproteome changes during mouse skin carcinogenesis. *Cell Rep* 3: 552−566

Zhao Y, Boguslawski G, Zitomer RS, DePaoli-Roach AA (1997) *Saccharomyces cerevisiae* homologs of mammalian B and B' subunits of protein phosphatase 2A direct the enzyme to distinct cellular functions. *J Biol Chem* 272: 8256−8262

Zuzuarregui A, Kupka T, Bhatt B, Dohnal I, Mudrak I, Friedmann C, Schüchner S, Frohner IE, Ammerer G, Ogris E (2012) M-Track: detecting short-lived protein-protein interactions *in vivo*. *Nat Methods* 9: 594−596